Ca^{2+} SIGNALING IN THE NEAR PLASMA MEMBRANE MICRODOMAIN OF NON-EXCITABLE CELLS

APPROVED BY SUPERVISORY COMMITTEE

Shmuel Muallem, Ph.D.

Ilya Bezprozvanny, Ph.D.

Donald Hilgemann, Ph.D.

Kristine E. Kamm, Ph.D.

Yi Liu, Ph.D.

To My Family

Ca^{2+} SIGNALING IN THE NEAR PLASMA MEMBRANE MICRODOMAIN OF NON-EXCITABLE CELLS

by

Jian Yao

DISSERTATION

Presented to the Faculty of the Graduate School of Biomedical Sciences

The University of Texas Southwestern Medical Center at Dallas

In Partial Fulfillment of the Requirements

For the Degree of

DOCTOR OF PHILOSOPHY

The University of Texas Southwestern Medical Center at Dallas

Dallas, Texas

December, 2010

Acknowledgements

I would like to thank my mentors, Dr. Shmuel Muallem, for providing an exciting environment for research; Dr Ilya Bezprozvanny, for guiding me through the final stage of preparing the dissertation.

I would like to thank the members of my committee, Drs. Kristine Kamm, Donald Hilgemann and Yi Liu for their insight and advice. I would also like to thank Dr Melanie Cobb for her inspiration. Without their encouragement, I would have been lost during this winding journey.

I would also like to thank the members of the Muallem lab who helped me extensively through the years. Xiang Luo, Qin Li and Guojin Huang have been tremendously helpful with my projects. Weizhong Zeng, Xinhua Wang and Abigail Soyombo provided helpful comments on the projects.

I thank my family and friends who never lose confidence in me. Without their supports it would be impossible for me to finish this dissertation.

Ca^{2+} SIGNALING IN THE NEAR PLASMA MEMBRANE MICRODOMAIN OF NON-EXCITABLE CELLS

Jian Yao

The University of Texas Southwestern Medical Center at Dallas, 2010

Supervising Professors: Shmuel Muallem, Ph.D.
Ilya Bezprozvanny, Ph.D.

Calcium is the most versatile second messenger and plays fundamental roles in orchestrating enzyme secretion in exocrine acinar cells. Previous studies in excitable cells demonstrated the existence of high Ca^{2+} microdomains. The major function of such microdomains is to create high local calcium concentration to activate various calcium-dependent signaling events. However, in non-excitable cells, direct evidence of such microdomains is absent. The goal of my study is to characterize the properties of high Ca^{2+} microdomains in acinar cells and explore its physiological relevance in the context of the secretory functions.

By combining Total Internal Reflection Fluorescence Microscopy (TIRFM) technique and wide-field fluorescence imaging, I was able to quantify and compare changes in the concentration of free Ca^{2+} in the near membrane microdomains ($\Delta[Ca^{2+}]_{PM}$) and in the bulk cytosol ($\Delta[Ca^{2+}]_{Cyto}$). $\Delta[Ca^{2+}]_{PM}$ is about 3-fold larger than $\Delta[Ca^{2+}]_{Cyto}$ under maximal agonist stimulation, while resting $[Ca^{2+}]_{PM}$ and $[Ca^{2+}]_{Cyto}$ shows no difference. Near membrane microdomains also showed greater Ca^{2+} influx following store depletion induced either by activating surface receptor or by inhibiting SERCA pump. In response to physiological strength of stimulation, Ca^{2+} oscillation in the two compartments showed significantly different dynamics.

The activation mechanisms of the Ca^{2+}-induced Ca^{2+} release (CICR) are well established in cardiac and skeletal muscles and involves high Ca^{2+} microdomains. My study was the first to demonstrate the presence of CICR in the parotid acinar cell. In these cells, minimal activation of Ca^{2+} influx by partially depleting the stores, either by directly activating the cell surface receptor or by inhibiting SERCA, leads to an explosive release of Ca^{2+} from the majority of the stores, mediated presumably by RyR away from microdomains.

The last part of my study is on the effects of chronic ER stress on Ca^{2+} signaling. The study suggests that ER stress induced by PERK mutation impeded both the efficiency and fidelity of Ca^{2+} signaling.

My work validates the existence of near plasma membrane microdomains in non-excitable exocrine cells. The fact that $[Ca^{2+}]_{PM}$ and $[Ca^{2+}]_{Cyto}$ differ in many ways suggests that microdomains is the central signaling platform in these cells.

Table of Contents

Prior Publications

1. Fredericksen BL, Wei BL, Yao J, Luo T, Garcia JV. (2002). Inhibition of endosomal/lysosomal degradation increases the infectivity of human immunodeficiency virus. *J Virol*. 76(22):11440-6.
2. Yao J, Li Q, Chen J, Muallem S. (2004). Subpopulation of store-operated Ca2+ channels regulate Ca2+-induced Ca2+ release in non-excitable cells. *J. Bio.l Chem.* 279(20):21511-9.
3. Huang G*, Yao J*, Zeng W, Mizuno Y, Kamm KE, Stull JT, Harding HP, Ron D, Muallem S. (2006). ER stress disrupts Ca2+-signaling complexes and Ca2+ regulation in secretory and muscle cells from PERK-knockout mice. *J Cell Sci.* 119(Pt 1):153-61. (* equal contribution)

List of Figures

List of Tables

List of Abbreviations

2-APB	2-aminoethoxydiphenyl borate
$[Ca^{2+}]_i$	concentration of calcium in the cell
$[Ca^{2+}]_O$	concentration of calcium outside the cell
$[Ca^{2+}]_{ER}$	concentration of calcium in ER
$[Ca^{2+}]_{PM}$	concentration of calcium in the near plasma membrane microdomain
$[Ca^{2+}]_{cyto}$	concentration of calcium in the bulk cytosol
cAMP	cyclic adenosine monophosphate
CCE	capacitative Ca^{2+} entry
CCK	cholecystokinin
CICR	Ca^{2+}-induced Ca^{2+} release
CPA	cyclopiazonic acid
DAG	diacylglycerol
ER	endoplasmic reticulum
FCCP	carbonylcyanide p-trifluoromethoxyphenylhydrazone
GPCR	G protein coupled receptor
Icrac	current by Ca^{2+}-release-activated Ca^{2+} channel
IP_3	inositol 1,4,5-triphosphate
IP_3R	inositol triphosphate receptor
MCU	mitochondrial Ca^{2+} uniporter
mNCX	mitochondrial Na^+-Ca^{2+} exchanger
mHCX	mitochondrial H^+-Ca^{2+} exchanger
PERK	interferon-inducible RNA-dependent protein kinase-like ER kinase
PIP_2	phosphatidylinositol (4,5)-bisphosphate
PLC-β	phospholipase C-β
PM	plasma membrane
PMCA	plasma membrane Ca^{2+} ATPase
RGS	regulator of G protein signaling
ROC	receptor operated Ca^{2+} channel
RyR	ryanodine receptor
SERCA	sarco/endoplasmic reticulum Ca^{2+} ATPase
SLO	streptolysin O
SOC	store operated channel
SOCE	store operated Ca^{2+} entry
TIRFM	total internal reflection fluorescence microscopy
TRP	transient receptor potential
UPR	unfolded protein response
VOC	voltage operated Ca^{2+} channel

Chapter 1 Introduction

1.1 Overview

Besides the vital role in mineralization of bones, Ca^{2+} is employed in signal transduction by virtually all cell types. It is the most versatile second messenger that plays key regulatory roles in numerous cellular processes, such as fertilization, cell division and apoptosis, immune response, muscle contraction and enzyme secretion (Berridge et al., 2000; Lodish, 1999).

The ubiquitous presence of calcium ion in cells and its sophisticated regulatory mechanism make it suitable as a universal secondary messenger. First, the lipid bilayer of the plasma membrane and other organellar membranes are nonpermeable to Ca^{2+}. There is about 10,000 fold concentration difference of free Ca^{2+} across the plasma membrane (~1.2 mM in the extracellular space compared to ~0.1 μM in the cytosol) (Berridge et al., 2000; Lodish, 1999). This chemical gradient makes the flow of Ca^{2+} possible. It is this membrane potential that drives the movement of extracellular Ca^{2+} into the cell through Ca^{2+}-permeable channels. Similar Ca^{2+} gradients exist across the membranes of other intracellular organelles, such as the mitochondria and endoplasmic reticulum (ER) (Rutter et al., 1998). Such steep calcium gradient across the plasma and organellar membranes endows the Ca^{2+} ion the ability to convey signals through regulated transport across the membranes.

Secondly, within the cell, only the free Ca^{2+} ion is the physiologically active form. The level of free intracellular calcium is maintained low through the regulation of two families of proteins, calcium transporters lining the plasma and organellar membranes and calcium binding/buffering proteins in the cytosol. Ca^{2+} transporters, including Ca^{2+}-permeable ion channels, Ca^{2+} pumps and Ca^{2+} related ion exchangers, facilitate rapid and regulated transport of Ca^{2+} across membranes. Ca^{2+} buffer molecules, existing in both cytosol and organelles, modulate the concentration of free calcium, adding another level of regulation of the Ca^{2+} concentration in the cell.

Thirdly, the Ca^{2+} concentration in the cell is neither static nor homogeneous. The signal-induced Ca^{2+} concentration changes are precisely regulated in both time and space. As a result, the temporal and spatial regulation of Ca^{2+} concentration is vital to the intensity and specificity of numerous cell signaling processes. A large number of genes and transcription factors are regulated by the intracellular Ca^{2+}. Ca^{2+} is also unique in that it modulates some of its own regulators, including inositol triphosphate receptor (IP_3R) and ryanodine receptor (RyR) (Berridge et al., 2003). Therefore, the dynamics of Ca^{2+} concentration can be regulated by various feedforward and feedback mechanisms.

It is critical for the cell to maintain proper concentration of Ca^{2+} in each compartment, disturbance of this homeostasis often results in cell damage. In fact, several pathological conditions have been attributed to over/underload of cytosolic or organellar Ca^{2+} (Arai et al., 1993; Mattson, 2010; Matute, ; Muller et al., 2006; Periasamy and Huke, 2001; Verkhratsky and Fernyhough, 2008). For the purpose of this introduction, I will briefly review the regulation of intracellular Ca^{2+} concentration of electrical non-excitable cells. The concept of Ca^{2+} microdomain will be introduced and the properties of individual

regulators in microdomains, their relationship with global Ca^{2+} changes and physiological significance will be discussed.

1.2 PM-ER Calcium Microdomain

Two decades ago, Llinas and colleagues first reported extraordinary high concentration of calcium that occurred only at particular spots (Llinas et al., 1992). By injecting a low affinity Ca^{2+}-sensitive photoprotein (n-aequorin-J) into the presynaptic terminal of giant squid synapse, Llinas was able to measure the local concentration of calcium ($[Ca^{2+}]_i$), as indicated by the intensity of light emission of n-aequorin-J. During the stimulation of synapse, the reading of light emission suggested that the calcium concentration could reach as high as 200~300 μM. Interestingly, high calcium spikes always formed at specific positions and remained in the same places.

Since then, the concept of Ca^{2+} microdomain has been used to describe a physically restricted (within 10-100 nm radius) and functionally distinguishable subcellular region in the cytoplasm. There are many microdomains in different parts of the cell. The molecular composition, size and life span may differ from microdomain to microdomain. In accordance with its function to elicit abrupt increase in local $[Ca^{2+}]_i$, a microdomain is always organized around Ca^{2+} channels. Immediately adjacent to the pore of Ca^{2+} channels, the increase of $[Ca^{2+}]_i$ can be on the order of hundreds of micromolar. The robust increase in $[Ca^{2+}]_i$ is capable of inducing significant physiological consequences, such as vesicle fusion with plasma membrane, which is unlikely to be activated by Ca^{2+} at the concentration recorded in the bulk cytosol after stimulation. Therefore, the concept of Ca^{2+}

microdomain emphasizes a localized drastic change, in contrast to the more averaged and global change in the cytosol.

Compartmentalization of intracellular Ca^{2+} and presence of various Ca^{2+} transporters are the molecular basis of Ca^{2+} microdomains. Each involved organelle has intrinsic calcium transporters that move calcium ion between the organellar lumen and the cytosol. All calcium channels, regardless of the different gating mechanisms, allow Ca^{2+} ion to flow down the electro-chemical gradients without consuming energy. By contrast, Ca^{2+} pumps/ATPases move Ca^{2+} ion against the electro-chemical gradients at the expense of ATP. To understand the dynamics of calcium microdomain, it is necessary to review the major calcium transporters residing in the membrane of several important calcium stores (see table 1). I will start with the molecules and complexes within the PM-ER microdomains, followed by discussion of the components of other microdomains as well.

Cellular Ca^{2+} store	**Direction of Ca^{2+} flow**	**Channel/transporter**	**Ligand**
ER	Into the cytosol	IP_3R	IP_3, Ca^{2+}
		RyR	cADPR, Ca^{2+}
	Into the ER	SERCA	ATP, Ca^{2+}
External medium	Into the cytosol	Icrac	STIM1, Ca^{2+}
		TRPC	
	Out of the cell	PMCA	ATP, Mg^{2+}
Mitochondrion	Into the cytosol	Na^+/Ca^{2+} exchanger	Ca^{2+}, H^+, $\Delta\Psi$
		H^+/Ca^{2+} exchanger	
	Into the mitochondria	Mitochondrial	Ca^{2+}
		Ca^{2+} uniporter(MCU)	
		mRyR	Ca^{2+}
Golgi	Into the cytosol	IP_3R	IP_3, Ca^{2+}
	Into the Golgi	SPCA	ATP, Ca^{2+}

Table 1-1 Summary of calcium transporters involved in Ca^{2+} flux into and out of major Ca^{2+} stores in non-excitable cells

1.2.1 GPCR and Associated Signalplex

Fig1.1 illustrated a typical Ca^{2+} signaling cascade in the pancreatic acinar cell. The receptor-mediated Ca^{2+} release is initiated by ligand binding to G-protein coupled receptor (GPCR). $G_{\alpha q}$ then activates membrane-bound phospholipase C-β (PLC-β), which in turn catalyzes the hydrolysis of a membrane phospholipid, phosphatidylinositol (4,5)-bisphosphate (PIP_2), into inositol 1,4,5-triphosphate (IP_3) and diacylglycerol (DAG). When IP_3 binds and activates its receptor (IP_3R), a Ca^{2+} channel located in ER membrane, Ca^{2+} is released from the ER store into the cytosol (Berridge, 1993; Kiselyov et al., 2003).

The activity of G protein is modulated by Regulator of G protein signaling (RGS). An RGS protein is a large protein with a conserved GAP domain that carries out the catalytic function. The function of its C-terminal domain is largely unknown. The N-terminal domain confers receptor recognition by binding to scaffold protein such as spinophilin that also binds to the third intracellular loop of GPCRs (Wang et al., 2005). The N-terminus of RGS may also interact directly with GPCRs. The interaction between RGS proteins and GPCRs regulates the strength of the signal transmitted by GPCRs to downstream effectors. RGS proteins act in a receptor-specific manner. It is possible to down-regulate a specific GPCR by up-regulating corresponding RGS proteins. The activities of RGS proteins are also regulated by lipids, phosphorylation and by scaffolding protein such as Homer 2 (Shin et al., 2003)

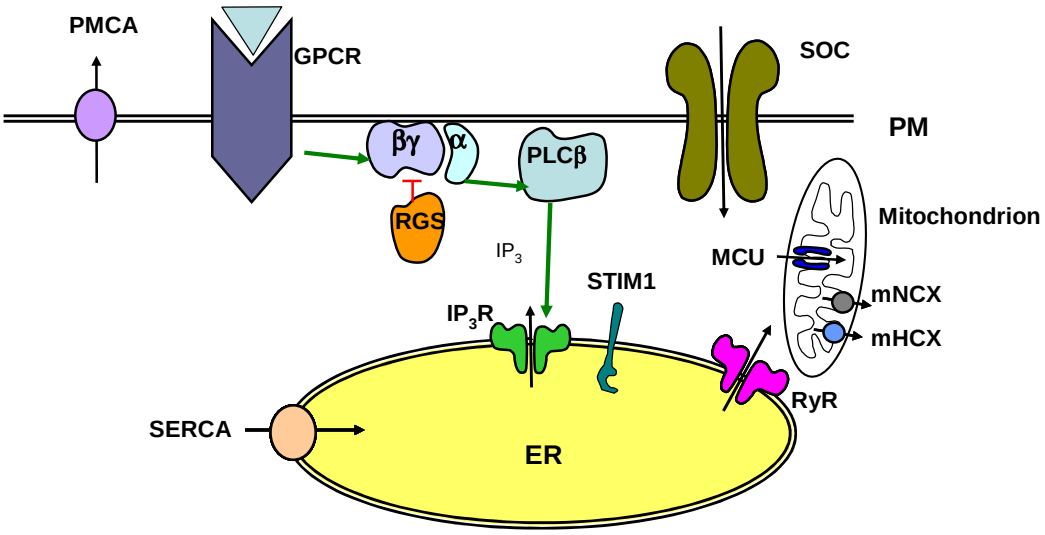

Figure 1-1 Schematic drawing of Ca^{2+} signaling in the pancreatic acinar cell.
Green lines indicate activation, red line indicates inhibition. Black arrows represent the direction of Ca^{2+} movement. PM, plasma membrane; PMCA, plasma membrane Ca^{2+} ATPase; GPCR, G-protein coupled receptor; SOC, store operated channel; PLC, phospholipase C; RGS, regulator of G-protein signal; ER, endoplasmic reticulum; SERCA, sarco/endoplasmic reticulum Ca^{2+} ATPase; IP3R , inositol 1,4,5-triphosphate receptor; RyR, ryanodine receptor; MCU, mitochondrial Ca^{2+} uniporter; mNCX, mitochondrial Na^{+}-Ca^{2+} exchanger; mHCX, mitochondrial H^{+}-Ca^{2+} exchanger.

1.2.2 IP_3 Receptors (IP_3Rs)

Before the discovery of IP_3 and its receptor, the mechanisms by which internal Ca^{2+} stores release Ca^{2+} in response to physiological stimulations have remained enigmatic. In the 1980s, IP_3 was the first molecular entity identified to mobilize Ca^{2+} from the internal stores (Berridge, 1993; Berridge et al., 1984; Streb et al., 1985). In 1990, the first IP_3 receptor was cloned as an ER membrane integral protein. Since then, three isoforms of IP3 receptor have been discovered. They all have six transmembrane spans and each isoform has its unique tissue distribution pattern (Bezprozvanny and Ehrlich, 1994; Bezprozvanny et al., 1991). IP_3R1 is found mainly in the brain. IP_3R2 is predominantly in the brain, heart and liver. IP_3R3 is in the pancreas, the kidney and the gastro-intestinal tract.

IP_3Rs are expressed in most mammalian cell types. It is found that more than one isoforms can co-express in one cell. IP_3 receptors function as either hetero- or homo-tetramers. Each monomer is encoded by one of the three IP_3R genes.

Each IP_3R monomer has six C-terminal transmembrane spans, the last two forming the pore of the channel. The ligand binding site for IP_3 is located at the N-terminus of the receptor. 7 of the 8 Ca^{2+} binding sites concentrate in the N-terminus and the regulatory domain that is between the C- and N-termini. This regulatory region also contains other recognition sites and binding surfaces for numerous regulatory peptides and small molecules, like Homer, Calmodulin, ATP and Caspase 3. The activity of the receptor is modulated by these molecules, whose abundance in turn, is regulated by various cellular processes. Thus, IP_3Rs function as an integrator of intracellular signal.

In principal, IP_3Rs are gated by both IP_3 and Ca^{2+}. However, given the diverse expression patterns and combinations of subunits in the receptor assemblies, it is not

surprising that the regulatory properties of IP_3R differ. As illustrated by the top view electronic microscope picture, 4 subunits clinch tightly. In the presence of IP_3, the subunits spread off from the center. It is suggested that the loosening of the structure increases the conductance of a channel. Interestingly, IP_3 gating of channels only occurs at optimum $[Ca^{2+}]_i$. Studies have shown that both low and high $[Ca^{2+}]_i$ inhibit IP_3R activation (Bezprozvanny et al., 1991).

Localization of IP_3Rs is equally critical in the gating of the channels. IP_3Rs are shown to express only underneath the luminal and lateral membrane, resembling the pattern of G-protein couple receptors such as CCK receptor and muscarinic receptor M3R (Lee et al., 1997; Shin et al., 2001). Co-localization greatly reduces the distance between the membrane receptors and the IP_3Rs and shortens the time that IP_3 needs to diffuse. As a result, the response time of the receptors to IP_3 is decreased while the sensitivity is increased. Thus the efficiency of the signal transduction is improved.

As it was clearly demonstrated, the expression of IP_3R in ER is highly polarized, reflecting the involvement of IP_3Rs in PM-ER Ca^{2+} microdomains. In addition to IP_3, other small molecules, such as PIP_2, DAG and cAMP, have also been implied in direct regulating IP_3Rs. The co-localization and interplay between the PM-ER receptors, channels and signaling molecules is referred to as PM-ER microdomain in these studies. Biotinylation of membrane proteins has revealed the expression of IP_3Rs in the plasma membrane. However, little is known about either the significance of IP_3Rs in the plasma membrane, or the regulatory interactions between GPCRs, Ca^{2+} pumps, IP_3Rs and RyRs.

1.2.3 Ca^{2+} Influx Channels

Ca^{2+} channel is the "entrance" in the membrane for Ca^{2+} ions. These channels, depending on their gating properties, can be categorized as voltage operated (VOC), store operated (SOC) or receptor operated Ca^{2+} channel (ROC). The presence of a particular type of channel often reflects the need to respond to a specific extracellular signal. For example, skeletal muscle cells possess a large number of L-type voltage gated Ca^{2+} channel, in accordance with the nature of the electrical signal that triggers muscle contraction. Upon activation by action potential, $Ca_V1.2$, a muscle specific VOC increases its permeability to Ca^{2+} and allows rapid influx of Ca^{2+} that eventually results in muscle contraction. On the other hand, in electrically non-excitable cells, store operated channels are responsible for the Ca^{2+} influx and play important roles in shaping the Ca^{2+} dynamics and regulating multiple cellular functions.

The receptor-mediated release of Ca^{2+} from IP_3-sensitive stores often triggers Ca^{2+} influx across the plasma membrane. Since such Ca^{2+} influx is due to decreased Ca^{2+} content in the stores, it is referred to as store-operated Ca^{2+} entry (SOCE) or capacitative Ca^{2+} entry (CCE). The channel that mediates the influx is known as store-operated Ca^{2+} channel (SOC). In addition to the activation of cell receptors, store depleting agents, such as thapsigargin and ionomycin, are also able to induce store-operated Ca^{2+} entry. SOCE is believed to play a critical role in replenishing the intracellular stores, therefore is essential for cellular processes depending on oscillatory Ca^{2+} transients.

Ca^{2+}-release-activated Ca^{2+} channel or Icrac channel is the best understood SOC channel at present (Hoth and Penner, 1992; Zweifach and Lewis, 1993). Pore-forming Orai1 was identified recently by using a siRNA screening (Yeromin et al., 2006). It was found that human patients with Orai1 lack Icrac current in theirT cells and suffered from

severe combined immunodeficiency disease. Expression of wild-type Orai1 restored Ca^{2+} influx in patient T cells. In addition, overexpression of Orai1 and STIM1 together markedly increases CRAC current. Recent studies also showed that the interaction between wild-type STIM1 and Orai1, assessed by co-immunoprecipitation, was greatly enhanced after Ca^{2+} store depletion. Moreover, site-directed mutagenesis in Orai1 resulted in altered ion selectivity of CRAC current. A charge neutralizing mutation of Orai1 acted as a dominant-negative non-conducting subunit. These accumulating evidences indicate that Orai1 itself mediates the Ca^{2+} conductance of SOC channel (Prakriya et al., 2006; Yeromin et al., 2006).

Members of the transient receptor potential (TRP) family are a subtype of SOC (Zhu et al., 1996). The *Drosophila* transient-receptor-potential (TRP) homologs were the first identified and intensively studied candidates as SOC subunit. Since their cloning two decades ago, members in the TRP family have attracted great interest in the Ca^{2+} signaling field. In cultured mammalian cells TRPC channels are activated through pathways that involving PLC. However, the mechanism through which the stimulation of PLC and the production of IP_3 potentiate the Ca^{2+} conductance of TRPCs remained elusive until the identification of STIM1 as ER Ca^{2+} sensor.

The role of TRP as SOC has been controversial from the very beginning. Early studies described SOCE/I_{crac} as inwardly rectifying, highly Ca^{2+}-selective, current that is blocked by Ni^{2+}, and exhibit characterization of voltage-independent gating. By contrast, electrophysiological properties of TRPC family channels are not associated with the above description. Now we know TRPC channels, like I_{crac} channels, are all subtype of SOC and are regulated by STIM1 (Cahalan, 2009; Worley et al., 2007).

SOC plays critical roles in the normal physiology of acinar cells. As mentioned before, the secretory function of acinar cells depends on the elevation of $[Ca^{2+}]_i$. Studies have shown that the release of secretory vesicles always occurs in a successive pulses manner preceded by oscillatory $[Ca^{2+}]_i$ increase. The oscillation of $[Ca^{2+}]_i$ will quickly diminish if the stores are not replenished promptly. In Ca^{2+} free environment, oscillation of $[Ca^{2+}]_i$ eventually stops despite the presence of stimulants. Refilling of Ca^{2+} stores by activation of SOC retains acinar cells capability of continuous secretion.

1.2.4 STIM1

Recently a RNA interference (RNAi)-based screen identified STIM1 as the sensor of the Ca^{2+} content in ER for SOCs. STIM1 is an ER membrane protein composed of multiple domains including a Ca^{2+} binding EF-hand motif, a sterile alpha motif (SAM), and a C-terminal coiled-coil for protein interaction (Cahalan, 2009). The N-terminus of the STIM1 is in the ER lumen while the C-termininus is located in the cytosol.

In resting state, intact STIM proteins heteromultimerize while isolated C-terminal and N-terminal ER-SAM domain form dimers and monomers respectively (Baba et al., 2006; Dziadek and Johnstone, 2007; Ji et al., 2008). When Ca^{2+} content in the ER lumen decreases, the EF-hand domain dissociates with Ca^{2+} and translocate to the plasma membrane, carrying with it the message of the ER has been depleted. Intact STIM1 form clusters called ‘puncta’ immediately adjacent to the plasma membrane. Moreover, clusters of STIM1 were found to concentrate at predetermined foci in the peripheral ER, positioning against the plasma membrane (Liou et al., 2007; Lur et al., 2009; Wu et al., 2006).

STIM1 interacts directly through its C-terminal with Orai and TRPC channels and activates them. Actually, the truncated C terminus alone is sufficient to constitutively activate I_{crac} current and TRPC1 channel regardless of the filling status of ER (Muik et al., 2008; Penna et al., 2008; Yuan et al., 2007; Zhang et al., 2008). The discovery of the important role of STIM1 in regulating Ca^{2+} influx channels has reshaped the concept of store operated channel. SOCs can be regarded as membrane channels that are regulated by STIM1 and require the translocation of STIM1 from ER to the plasma membrane in response to depletion of the ER Ca^{2+} stores (Cahalan, 2009; Worley et al., 2007).

1.2.5 Ryanodine Receptors (RyRs)

Ryanodine receptor (RyR) is another major family of intracellular Ca^{2+} channels. Functional RyRs comprise four identical subunits. Each subunit has a large N-terminus that protrudes to the cytosol and contains multiple recognition sites for kinases, phosphatases, nucleotides and peptides.

In mammalian cells there are three isoforms of RyR, namely, RyR1, RyR2 and RyR3. Each isoform has its unique tissue distribution pattern. RyR1 is mainly expressed in the skeletal muscles. RyR2 is mainly expressed in the cardiac muscle. RyR3 is ubiquitously expressed in the brain, the muscles and the pancreas. In muscle, RyRs are expressed exclusively on the sarcoplasmic reticulum and are a critical mediator of excitation-contraction coupling (E-C coupling). At least some of the RyRs are located in close proximity to the L-type voltage gated Ca^{2+} channel in the sarcoplasmic membrane of the transverse tubules. This sarcoplasmallemel-SR microdomain harbors the machinery to convert electrical pulse to intracellular Ca^{2+} increases. When L-type channel is activated, it undergoes conformational change that leads to initial Ca^{2+} influx. This initial wave of Ca^{2+}

activates RyRs and the subsequent Ca^{2+} release from activated RyRs further evoke more Ca^{2+} release from the neighboring RyRs. Thus, the initial signal is transmitted and amplified to trigger muscle contraction. This cascade of Ca^{2+} releasing evens is termed Ca^{2+} induced Ca^{2+} release (CICR). E-C coupling is a good example of how microdomains coordinate rapid and precisely controlled Ca^{2+} dependent processes by selectively coupling different cellular signaling pathways to different Ca^{2+} entries.

RyRs are also widely expressed in non-muscle cells. All three RyRs have been found in the brain. RyR2 was also found in the pancreatic acinar cells. RyR3 and a splice form of RyR1 were also cloned from the parotid acinar cells (Fitzsimmons et al., 2000; Lee et al., 2002; Straub et al., 2000). However, the functions of RyRs in these non-excitory tissues are still under investigation.

Ca^{2+} is not the only endogenous ligand for RyRs. NAADP and cADP-ribose have all been proposed as physiological activators of the channels since these two molecules may be involved in CICR pathways. However, the physiological validation of these molecules as RyR ligand is still evasive. In addition to the debate on whether RyRs are the internal receptors of these messengers, the enzymatic pathway responsible for the synthesis and the degradation of them are not clear either. Moreover, the apparent involvement of cAMP/cGMP in the metabolism of cADPR and NAADP seems to bring the G proteins and GPCRs into the complexity of the PM-ER microdomains (Lee, 2000; Lee, 2004).

1.2.6 Sarco/Endoplasmic Reticulum Calcium ATPase (SERCA)

Even small fluctuations of $[Ca^{2+}]_i$ affect numerous downstream molecules that are regulated or modulated by Ca^{2+}, let alone a long lasting rise in $[Ca^{2+}]_i$ of big magnitude.

Excessive Ca^{2+} could induce cytotoxicity that may result in apoptosis. Hence, it is crucial for all the cytoplasmic organelles to function in a highly cooperative manner to clear the free Ca^{2+} ions after their work is done in the cytosol. Since the elevated $[Ca^{2+}]_i$ is still much lower than $[Ca^{2+}]_O$ and $[Ca^{2+}]_{ER}$, it requires Ca^{2+} pumps to extrude Ca^{2+} from the cytosol at the expense of ATP hydrolysis.

There are three isoforms of Sarco/Endoplasmic reticulum Ca^{2+} ATPases (SERCAs) in mammalian cells, including SERCA1, SERCA2 and SERCA3. They are encoded by three genes, ATP2A1, ATP2A2 and ATP2A3, respectively. More variants are generated by alternative splicing. The three major isoforms of SERCA differ in Ca^{2+} affinity, turnover rate and tissue distribution. SERCA1 and SERCA2a are muscle specific isoforms, whereas SERCA2b is expressed ubiquitously, including in the epithelium. In acinar cells the expression pattern of SERCA was reported to be polarized. Immunohistochmistry showed that in pancreatic acinar cells, SERCA2a is expressed in the luminal pole and SERCA2b is expressed in the basal pole and on the nuclear envelop. In contrast, in the submandibular acinar cells, SERCA2b was found in luminal pole and SERCA3 was found in the basal pole (Lee et al., 1997). Knocking out specific subtypes of SERCA revealed the distinct role of each SERCA isoform and functional redundancy of critical proteins (Ahn et al., 2003).

1.2.7 Plasma Membrane Ca^{2+} ATPase (PMCA)

Plasma membrane Ca^{2+} ATPase (PMCA) is responsible for removing Ca^{2+} from the cytosol to the extracellular space. PMCA molecule is a single chain protein with 10 putative transmembrane spans. The activity of PMCA is modulated by $[Ca^{2+}]_i$. When $[Ca^{2+}]_i$ rises, Ca^{2+}-bound calmodulin and acidic phospholipids such as PIP_2 increase the

affinity of Ca^{2+} for PMCA. The K_m goes down to 0.2 μM, compared to 10 μM at resting state. When PMCA is activated, it pumps Ca^{2+} across the plasma membrane against the chemical gradient at the expense of ATP hydrolysis.

Since prolonged elevation of $[Ca^{2+}]_i$ is cytotoxic, it is vital for PMCA to act promptly to remove excessive cytosolic Ca^{2+}. Undesired changes in the expression of PMCA and consequent disturbance of Ca^{2+} homeostasis may result in fatality or disease. Mutants in PMCA are associated with diseases including cataract formation, carcinogenesis, cardiac hypertension and hypertrophy. On the other hand, due to the expression redundancy and function overlap, severity of these diseases is determined by the expression pattern of the PMCA isoforms in the specific tissue affected (Brini and Carafoli, 2009; Wu et al., 2009).

1.3 *ER-Mitochondrial Calcium Microdomain*

The concept of Ca^{2+} microdomains is not restricted to the region proximate to the ER and plasma membrane. In fact, functional Ca^{2+} microdomains exist in different sub-cellular locations where action of Ca^{2+} is tightly regulated by its release and uptake. Although my research in this dissertation focuses on the near plasma membrane microdomains, it is necessary to summarize the characteristics of other microdomains briefly because the microdomains interplay and the cellular Ca^{2+} homeostasis depends on collective action of these functional modules.

Also known as the “power plant” of the cell, mitochondrion is another Ca^{2+} storage that plays an indispensable role in regulating $[Ca^{2+}]_i$. Mitochondrion is known to buffer

and store Ca^{2+} in its matrix and the Ca^{2+} transporting components in the mitochondrion include ion exchanger and mitochondrial uniporter (see table 1). At rest state, $[Ca^{2+}]_{Mito}$ is maintained at 0.5 mM. $[Ca^{2+}]_{Mito}$ was shown to rise following IP_3 mediated $[Ca^{2+}]_i$ elevation. On the other hand, $[Ca^{2+}]_{Mito}$ did not respond to induced $[Ca^{2+}]_i$ elevation by perfusing permeabilized cell with Ca^{2+}. The fact that mitochondria distinguishes between physiological Ca^{2+} release and artificial Ca^{2+} elevation raised the speculation that certain mitochondria may position themselves in close proximity to the Ca^{2+} releasing channels. If the mitochondrial Ca^{2+} uniporter co-localizes with ER Ca^{2+} channels to form functional microdomains, these mitochondria will be exposed to extraordinary high $[Ca^{2+}]_i$ during activation, which would be absent elsewhere in cells. Thus, artificial Ca^{2+} elevation by perfusing will not generate localized high $[Ca^{2+}]_I$ that is capable of evoking Ca^{2+} flux through mitochondrion. Such mechanism will ensure both the efficiency and specificity of the signaling.

This hypothesis is supported by experimental data demonstrating that the extracted mitochondria actually had very low affinity for Ca^{2+} with K_d around 1 μM. They would not be able to play any essential role in Ca^{2+} homeostasis under normal $[Ca^{2+}]_{Cyto}$ concentration unless they are placed in microdomains with high $[Ca^{2+}]_i$. EM imaging showed that mitochondria and ER are indeed located in close proximity to each other(Rizzuto et al., 2004). It was evident that in living Hela cells, some mitochondria and ER lied within 100nm of each other (Rizzuto et al., 1998). Such distance falls into radius of a microdomain. Moreover, study by Park et al. demonstrated that in pancreatic acinar cells, mitochondria form three circular structures surrounding nucleus and secretory granules, and underlining the plasma membrane (Park et al., 2001). It was speculated that

with such a distribution pattern, the mitochondria reside next to or in contact with specific Ca^{2+} channels and Ca^{2+} pumps of these cellular compartments.

In addition to their function to buffer $[Ca^{2+}]_i$, mitochondria also rely on increased $[Ca^{2+}]_{Mito}$ to boost the energy production. This is a critical process because cells need extra energy in the form of ATP, to exclude Ca^{2+} from the cytosol, either back to ER by SERCA or out of the cell by PMCA. It has been shown that in Hela cells, the activity of PMCA is modulated by the subplasmalemmal mitochondria (Frieden et al., 2005). The mitochondria microdomains allow transport of molecule occur in a highly efficient manner.

Mitochondria also play critical roles in shaping the Ca^{2+} waves and oscillations. When the membrane potential of mitochondria was ablated by FCCP to disrupt mitochondrial Ca^{2+} uptake, the pattern of the propagation of the Ca^{2+} wave in acinar cell was significantly altered (Park et al., 2001).

1.4 Pancreatic and Parotid Exocrine Acinar Cells

In this study, I used pancreatic and salivary parotid acinar cells to study the regulation of intracellular $[Ca^{2+}]_i$. Acinar cells are glandular epithelial cells specialized for exocrine secretion. Exocrine pancreas is responsible for massive digestive enzymes production and secretion.

Cytoplasm of an acinar cell is visibly polarized. The electron microscope image in Figure 1.2 shows part of an exocrine pancreatic acinus with a typical wedge-shaped acinar cell at the center. The apical pole (also called luminal pole) is enriched in secretory vesicles (mature zymogen granules). The basal pole at the opposite end of the cell hosts the nucleus and protein synthetic organelles (ribosome on rough endoplasmic reticulum). The Golgi apparatus and immature secretory vesicles (condensing vacuoles) are usually

located midway along the cell. Based on this arrangement, the direction of protein synthesis and secretion is from basal to apical pole. The basal-lateral membrane is separated from the apical membrane by tight junctions that prevent the diffusion of substances between the luminal fluid and the interstitial fluid. A cluster of acinar cells form a corona-like acinus around the lumen.

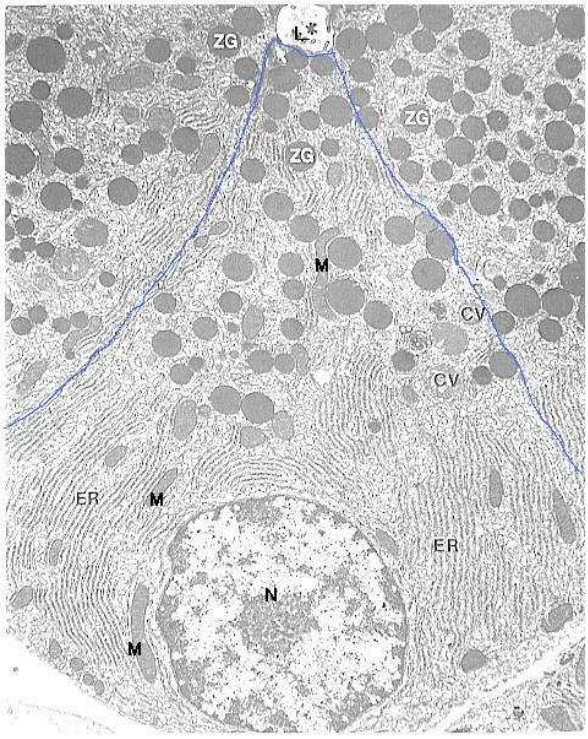

Figure 1-2 Electron microscope image of a pancreatic acinar cell.
The border of a wedge-shaped cell is outlined in blue. CV, condensing vacuole; ER, endoplasmic reticulum; L, lumen of acinus; M, mitochondrion; N, nucleus; ZG, zymogen granule; 15,000 X
Source of image: http://dspace.udel.edu:8080/dspace/handle/19716/1649

Acinar cells have been of great value to the study of Ca^{2+} signaling since the discovery of the intracellular Ca^{2+}-releasing function of inositol 1,4,5-trisphosphate (IP_3) in the pancreas (Streb et al., 1985; Streb et al., 1983). Pancreatic acinar cell is activated by both neurotransmitters such as acetylcholine and hormones including bombesin and cholecystokinin. Upon activation of the cell, the calcium dynamics demonstrate different patterns depending on the strength and duration of the stimulation. For example, low concentration of cholecystokinin (CCK) at 10^{-11} M often induces oscillatory $[Ca^{2+}]_i$ rises while 10^{-7} M of CCK induces robust and sustained $[Ca^{2+}]_i$ increase. Interestingly, the agonist-induced global rise of $[Ca^{2+}]_i$ occurs in a polarized manner. It initiates from the apical pole and propagates through the cell to reach the basal pole, a phenomenon termed Ca^{2+} wave.

The polar nature and versatility of Ca^{2+} signaling makes acinar cells a popular study object. It is well known that intracellular $[Ca^2+]_i$ play critical regulatory roles in every step in protein production and secretion. A considerable amount of data has been accumulated on the regulation of Ca^{2+} signaling in acinar cells, including the activation of surface receptors, release of $Ca^{2+}$from the internal stores, Ca^{2+} flux across cell membrane, $Ca2^+$ transients-associated secretion and the involvement mitochondria (Berridge et al., 2003; Kiselyov et al., 1999; Kiselyov et al., 2002; Kiselyov et al., 2006; Park et al., 2001; Shin et al., 2001; Straub et al., 2000; Thorn, 1993). Thus pancreatic acinar cells have become one of the best-characterized models of Ca^{2+} signaling.

1.5 Aims of this Dissertation Research

The research work described in this dissertation involves three major parts: 1) comparative studies of the differentially regulated $[Ca^{2+}]_{PM}$ and $[Ca^{2+}]_{Cyto}$ dynamics using

TIRFM and WFM respectively in the pancreatic acinar cells; 2) study of the regulatory mechanisms of Ca^{2+}-induced Ca^{2+} release (CICR) in the parotid acinar cell; 3) evaluation of the effects of the ER stress and disruption of the microdomain architecture on the regulation of $[Ca^{2+}]_i$.

Chapter 1 gives a literature overview of the calcium signaling with emphasis on the introduction of the concept of calcium microdomains.

Chapter 2 presents the methods utilized in this research. Some theoretical background of the TIRF microscopy method is also introduced.

Chapter 3 uses TIRF to study the PM/ER microdomain.

Chapter 4 studies the Ca^{2+}-induced Ca^{2+} release (CICR) in the parotid acinar cell.

Chapter 5 discusses the integrity of membrane signaling microdomain is essential to Ca^{2+} regulation.

Chapter 6 summarizes the work described in the preceding chapters and provides thoughts on alternative studying approaches and future directions.

Chapter 2 Experimental Procedures

2.1 Material

2-aminoethoxydiphenyl borate (2-APB), SKF96365 and ionomycin free acid were from Calbiochem. Cyclopiazonic acid was from Alomone labs (Jerusalem, Israel). CCK-8 was from Research Plus (Boston, MA). 1,4,5-$InsP_3$ was from Alexis Biochemical (San Diego, CA). Bovine serum albumin and protease inhibitor cocktail were from Roche. Carbamoylcholine chloride, heparin, sodium pyruvate, soybean trypsin inhibitor and other general chemicals were from Sigma. Anti-IP_3R3 antibodies were from Transduction labs.

The standard bath solution A contained: 140 mM NaCl, 5 mM KCl, 1 mM $MgCl_2$, 1 mM $CaCl_2$, 10 mM HEPES (pH 7.4, adjusted with NaOH) and 10 mM glucose. Solution A was supplemented with 10 mM sodium pyruvate, 0.02% (w/v) soybean trypsin inhibitor, and 1 mg/ml bovine serum albumin to compose the solution that was used for gland digestion and named PSA.

Ca^{2+}-free solution was prepared by omitting $CaCl_2$ from and supplementing with 0.2 mM EGTA to solution A. Ca^{2+} concentration in solution A was adjusted between 0.5-7.5 mM by addition of appropriate amount of 1M $CaCl_2$.

2.2 Preparation of mouse parotid acini and single acinar cells

Mouse parotid acini and single cells were prepared immediately before experiments. The animal used in this study was female C57BL/6 mouse, 20~22g of body weight (Charles River Laboratories). For experiments that involve comparisons between

normal and mutant cells, I used mice that carry homo/heterogeneous mutation and their wild type litter mates as control.

To prepare multiple cell acini, the animal was sacrificed by cervical dislocation. The skin was then opened at throat following cleaning of the area with 70% alcohol. The parotid glands were detached between the ear cartilage and the cheek. Removed glands were washed with PSA and then minced finely with dissection scissors.

The tissue was transferred to a 25 ml flask and suspended in PSA containing 0.3 mg/ml collagenase P (Roche Applied Science). The flask was gassed with 95% O_2— 5% CO_2, capped and secured in a 37°C shaking water bath. After 5 min of agitation, the tissue was partially dispersed by pipetting with a 5ml plastic pipette tip and digestion continued for an additional 3-4 minutes till the chunks of tissue disappeared.

The digested tissue was washed twice with PSA in 50ml centrifuge tubes by spinning down at 1000g for 1 min. The cell suspension was then filtered through a 75 μm nylon mesh to remove large pieces of tissue. After a final spin, the pellet of acini was re-suspended in 10ml PSA and kept on ice before experiments.

For Ca^{2+} wave recording purpose, the parotid glands were minced and washed once with Ca^{2+}-free solution A. The tissue was re-suspended in 5ml solution containing 0.025% (w/v) trypsin. This solution was prepared by a 1:1 dilution of a trypsin/EDTA solution (Sigma) with PBS (Gibco). The tissue was transferred to a 25 ml flask and incubated at 37^{o}C for 7 min in a gently shaking (<80 rpm) water bath.

Trypsin treatment was terminated by washing the cell twice with PSA. The tissue was then re-suspended in 5ml PSA containing 0.3 mg/ml collagenase P and the

flask was gassed with 95% O_2— 5% CO_2, capped and incubated at 37°C for 7 min while shaking agitatedly.

After the digestion, the cells were washed with PSA twice, filtered through a 75 μm nylon mesh. The pellet of single cells was re-suspended in 10ml PSA and kept on ice.

2.3 Preparation of mouse pancreatic acini and single acinar cells

Mouse pancreatic acini were prepared immediately before experiments. Mouse was sacrificed by cervical dislocation. The abdomen was then opened following a cleaning of the skin with 70% alcohol. The pancreas was located under the stomach and in close association with the spleen and duodenum. The removed tissue was soaked with PSA using a 27 gauge needle. This practice ensured a maximum exposure of acini to trypsin inhibitor to prevent the pancreas from self-digestion.

To prepare multiple cell acini, the pancreas was minced finely with dissection scissors and suspended in 5ml PSA containing 0.3mg/ml collagenase P. The tissue was transferred to a 25ml flask, then the flask was gassed with 95% O_2— 5% CO_2 and capped. The suspension was agitated at 37 °C for 7~8 minutes till the chunks of tissue disappeared.

The dispersed tissue was washed with PSA twice, filtered through a 75 μm nylon mesh, spun down and re-suspended in 10ml PSA. The cells were kept on ice before experiment.

For Ca^{2+} wave recording purpose, single pancreatic acinar cells were prepared in a similar manner as parotid cells were, only with shorter trypsin digestion (3 min) and collagenase P (5 min) digestion.

2.4 Load acinar cells with fluorescent calcium indicators

Fura-2 AM and Fluo-3 AM were purchased from TEFlabs (Austin, TX). Calcium green-1 AM and Pluronic acid F127 were from Molecular Probes (Eugene, OR). All fluorescent calcium indicators in the form of acetoxymethyl easter (AM) were dissolved in DMSO to make stock solution at concentration of 5mM. Aliquots of 2 µl of the stocking solutions were kept at -20°C. A stock solution of 20% (w/v) Pluronic acid F127 (a permeability enhancer) was made by dissolving Pluronic acid in DMSO at 40 °C.

Acinar cells were washed once with and suspended in Solution A. The serum contents in PSA may lower the loading efficiency. Transfer 1ml of cell suspension to a new 50ml centrifuge tube. Add 2 µl of pluronic acid stock solution and 2 µl florescent Ca^{2+} indicators stock solution to the same tube, giving a final concentration of 0.04% (w/v) Pluronic acid and 10µM indicators.

The cells were incubated in a 37°C water bath in darkness for 20 minutes. After loading, the acinar cells were spun down and re-suspended in 1ml PSA. The cells were ready to be examined by florescence microscopy and should be kept on ice throughout the experiments.

2.5 Fluorescence microscopy

Fluorescence microscope system integrates an epi-fluorescence system and a laser TIRF system. It consists of a Nikon Eclipse TE2000-U inverted microscope, Xenon light, a Sutter DG4/5 wavelength controller composed of dichroic mirrors/barrier filters, a Sutter illumination controller and a Roper Scientific Cascade CCD camera. A blue laser was used as a light source (10 mW 488nm Ion Laser by Spectra-Physics). A TIRF attachment is mounted to the optical pass of the microscope. This device allows the laser

beam to be steered before entering the objective. A Nikon oil immersion 60X Plan Apo TIRF objective (N.A.=1.45) is used to obtain TIRF images.

The following method was used to determine that the incidental light is total internal reflected (TIR). First, set the wide field fluorescence image of an acinus to desired intensity and then move the objective closer to the coverslip for about 0.1-0.2 μm. The incidental angle of the laser beam was steered larger until the brightness of fluorescence sharply decreased and the focus was adjusted to optimize the imaging. TIR was further confirmed using Bertrand lens, which allows examination of illumination at the back focus plane of the objective. When TIR was achieved the center of the focal plane became dark, leaving only an annular outskirt to be illuminated. Because the wide field fluorescence is much brighter than TIRF under the same laser power, neutral density filters were inserted in the optical pass to reduce the intensity of the wide field fluorescence to be comparable to that of the TIRF when simultaneous recording is needed.

All TIRF measurements were performed at 37°C on pancreatic acini consisting of 3-5 cells. Acinar cells loaded with Fluo-3 were plated on a poly-L-lysine coated cover slip, which was mounted at the bottom of a perfusion chamber. Images were acquired and analyzed using MetaFluor software (Universal Imaging). Unless otherwise stated, the speed of acquisition was 1 frame / sec.

$[Ca^{2+}]_{PM}$ was determined from the calibration of the fluorescence signals. After the designated treatment, the cells were exposed to 5 μM ionomycin in Ca^{2+}- free PSA containing 10 mM EGTA. When the signal stabilized, the cells were perfused with 5 μM ionomycin and 10 mM Ca^{2+} to saturate the dye. Ca^{2+} concentration was calculated using the following calibration equation.

$$[Ca^{2+}] = K_d \left(\frac{F - F_{min}}{F_{max} - F} \right)$$

K_d is the dissociation constant of a dye for calcium binding. F is the fluorescence intensity at any given time during the experiment; F_{min} and F_{max} are the fluorescence intensity of free and Ca^{2+}-saturated dye respectively in the presence of ionomycin. The K_d for Fluo-3 was assumed to be 390 nM. (Handbook, Molecular Probes) Results were reported as the mean ± S.E. of the indicated number of experiments. Student t-test was used for statistical analysis.

When cytosolic $[Ca^{2+}]_i$ was the only subject under investigation, it was measured by imaging pancreatic and parotid acini that were loaded with ratiometric dye Fura-2. Ratiometric indicators have significant advantages over single wavelength indicators in measuring $[Ca^{2+}]_i$. Their fluorescence signals depend solely on $[Ca^{2+}]_i$, and do not change with the loss of indicators from cell or the changes in cell shape. The recording system consists of a photomultiplier coupled to a microscope, a dichroic mirror and bandwidth filters, a PTI image acquisition and analysis system.

Fura-2 was excited alternately at two wavelengths of 355 nm and 380 nm; the emission of 510 nm was monitored. The ratio of the emission was expressed as: $R = F_{355} / F_{380}$. $[Ca^{2+}]_i$ were determined using the following calibration equation.

$$[Ca^{2+}] = K_d \left(\frac{R - R_{min}}{R_{max} - R} \right) \left(\frac{S_{f2}}{S_{b2}} \right)$$

The Kd for Fura-2 is assumed to be 224 nM. R_{min} and R_{max} are the fluorescence ratio of free and Ca^{2+}-saturated respectively. S_{f2} and S_{b2} are the fluorescence intensities of free and Ca^{2+}-bound dye at 380 nm only (Grynkiewicz, G et al, 1985).

The same PTI image system with 100X objective was use to analyze Ca^{2+} wave.

Fura-2 loaded acini clusters of 2-4 cells were chose for measurement. Fluorescence signal with single excitation at 380 nm was recorded at a speed of 30 frame/sec for 30 seconds. A bright field image of the same cell was taken and superimposed with fluorescence images so that the origin of Ca^{2+} wave could be determined.

To measure Mn^{2+} influx, Fura-2 loaded parotid acinar cells were recorded at an excitation wavelength of 360 mm. After exposure to Ca^{2+}-free PSA for 2 min, the cells were treated with the appropriate agonist for 2.5 min, and then were perfused with Ca^{2+}-free PSA supplemented with the agonist and 0.5 mM $MnCl_2$. The rate of quenching of Fura-2 fluorescence was determined by the slope of the quenching curves. Results were reported as the mean±S.E. of the indicated number of experiments.

2.6 Measurement of IP_3 production

To measure the yield of IP_3 by acinar cells, a competitive binding assay using radio labeled IP_3 was performed.

The basic buffer B contained: 100 mM NaCl, 50 mM Tris-base and 2 mM EDTA, pH was adjusted to 8.5 with concentrated HCl. Digested acini were spun down and re-suspended in solution B of desired volume (200 µl per sample).

Acinar cells were pipetted into individual eppendorf tube to mix with the preloaded agonists. In general, the acini were given 10 seconds at room temperature to activate and produce IP_3. To examine the reaction dynamics of the agonists, the reaction time was adjusted according to the design of experiments. The reactions were terminated by adding 20µl 20% perchloric acid to precipitate the proteins. The incubation was kept on ice for 20 minutes.

The mixture was centrifuged at 13000 RPM for 5 min. The supernatant was transferred to a new eppendorf tube. IP_3 was extracted by adding 20 μl 0.1M EGTA, 0.6 ml tri-n-octyl-amine and trichlorotrifluoroethane 1:1 (v:v) mixture to the supernatan. The tubes were vortexed to mix the reagents.

The layered mixture was centrifuged at 13000 RPM for 5 min. The upper layer contained IP_3 and was saved. 40 μl IP_3 containing sample was transferred to a new tube followed by addition of 40μl bovine cerebellum microsome and 30 μl ^3H-IP_3 (1:100 dilution of original in solution B, 10μl count~1000cpm). The total volume was brought to 200 μl by solution B.

A serial dilution of IP_3 was used to construct a standard curve. 40 μl of such IP_3 solutions replaced the 40μl IP_3 containing sample in the binding mixture described above.

The binding mixture was incubated at room temperature for 30 min before it was centrifuged at 13000 RPM for 3min. The supernatant was discarded and the pellet was washed with 200 μl solution B. At last, the pellet was re-suspended with 200 μl hot water (~60°C) and transferred to a scintillation vial together with 3ml scintillation solution (CytoScint TM from ICN) for radioactivity reading in a scintillation counter.

2.7 Immunocytochemistry

Dispersed acini were allowed to attach to glass microscope slides that were pre-treated with 0.01% poly-l-lysine at room temperature. The cells were permeabilized with methanol for 10 minutes at –20°C and then were washed twice with PBS. 5% goat serum diluted in PBS containing 1% bovine serum albumin and 0.1% gelatin (blocking buffer) was used to block the nonspecific antibody binding sites. After 1 hour of incubation, the

blocking buffer was replaced with 50 μl blocking buffer containing control serum or 1:100 dilution of anti-IP_3R1, anti-IP_3R2 or anti-IP_3R3.

The cells were incubated with primary antibodies overnight at 4°C to improve binding. After three washes with the blocking buffer, the cells were incubated with goat anti-rabbit IgG conjugated with Fluorescein or Rhodamine for 2 hr at room temperature. Finally, the cells were washed three times; let dry and sealed under cover slips with non-fluorescent mounting medium. Fluorescent images were collected with a Bio-Rad MRC 1024 confocal microscope.

2.8 Measurement of IP_3 mediated calcium release in SLO-permeabilized cells

To examine the potency of Ca^{2+} releasing channels located in ER, I used streptolysin O (SLO) to permeabilize the plasma membrane to allow exogenous IP_3 to enter the cell and mobilize Ca^{2+} from ER.

Derived from bacteria, SLO is a protein capable of binding to cholesterol and forming pores in the cell membrane. Since at 0°C SLO will only bind to cholesterol but will not form pores, if unbound SLO is removed from the medium before the temperature is raised to 37°C, only plasma membrane will be permeabilized. Therefore, SLO is very useful to create pores in the plasma membrane but leave internal organelles intact. The SLO permeabilization method allows access to internal organelles while avoiding the extensive extractions steps and potential harms to the membranes.

The dispersed acinar cells were washed twice with a high potassium solution (145mM KCl, 10mM HEPES and pH 7.4) and once with the same solution treated with Chelex 100 (Sigma). The cells were transferred to a fluorometer cuvette containing

warm incubation medium composed of the Chelex-treated solution, an ATP-regenerating system composed of 3mM ATP, 5 mM MgCl2, 10 mM creatine phosphate, 5 U/ml creatine kinase, a cocktail of mitochondrial inhibitors, 2 μM Fluo-3 (pentaammonium salt from Molecular Probes) and 3 mg/ml streptolysine O (SLO).

The excitation wave length of the fluorometer was set at 488 nm and the emission light was measured at 530 nm. It will take 2 to 5 min for $[Ca^{2+}]_i$ to stabilize due to the uptake of Ca^{2+} into the ER. Then IP_3 was added to the medium in increasing concentrations to mobilize Ca^{2+} from the ER. A mini-stirrer was placed in the cuvette to facilitate the diffusion of IP_3 and to prevent the acini from precipitating. At last, a high dose of 5 μM of IP_3 was added to the medium.

2.9 Measurement of contraction in urinary bladder smooth muscle strips

To prepare urinary bladder smooth muscle strips, the bladder was removed from a euthanized mouse and kept in solution B, 120.5 mM NaCl, 4.8 mM KCl, 1.2 mM $MgSO_4$, 1.2 mM NaH_2PO_4, 20.4 mM $NaHCO_3$, 1.6 mM $CaCl_2$ and 10.0 mM Glucose (pH 7.4) under room temperature. The wall of the bladder was cut open lengthwise; the bladder was flatted on the dissecting surface with lumen facing up. Then the urothelium was dissected off from the muscle layers.

The sheet of the bladder muscle was cut transversely into 3 equal width strips. The strips measured about 0.5x2.0x8.0 mm. The strips were tied up at both ends with surgical thread, one end fixed to the bottom of incubation chamber and the other end fixed to the lever arm of myograph recorder. The muscle strips were stretched to their full length and incubated in solution B, which was gassed with 95% O_2 and 5% CO_2.

Solution in the chamber was kept at 37 °C by the water circulating between the inner and outer walls of the chamber. High-K^+ solutions were prepared by isosmotic replacement of NaCl with KCl.

Chapter 3 Study of ER/PM Ca^{2+} Microdomain Regulation by TIRF

3.1 Background

The receptor-evoked Ca^{2+} signaling process is not uniform throughout the cytoplasm, in particular in the polarized cells. Stimulation of these cells results in Ca^{2+} oscillations, Ca^{2+} waves and localized changes in $[Ca^{2+}]_i$ (Thorn, 1993). To generate such complex and precisely regulated forms of Ca^{2+} signals, Ca^{2+} dynamics has to be regulated in discrete cellular microdomains. In addition, high local $[Ca^{2+}]_i$ are important for certain cellular functions, such as exocytosis (Neher, 1998). Indeed, recent evidence provided direct and indirect evidence for agonist-generated Ca^{2+} microdomains (Rizzuto and Pozzan, 2006). Direct measurement using a modified Ca^{2+}-sensitive photoprotein aequorin that is targeted to the plasma membrane, or the indirect measurement of Ca^{2+}-activated K^+ current and the Ca^{2+} dependence of neurotransmitter release have revealed the existence of specialized, high Ca^{2+} microdomain within a short distance from the PM (Marsault et al., 1997; Schneggenburger and Neher, 2000; Young and Zhang, 2004). The Ca^{2+} transients in this rim of cytoplasm termed near membrane microdomain or subplasmalemmal microdomain could be 10-100 folds higher than in the bulk cytosol.

The concept of near membrane Ca^{2+} microdomain depicts a temporally and spatially confined sub-membrane structure of macromolecular assemblies situated in immediate vicinity of Ca^{2+} release and/or influx channels. Theoretically, such Ca^{2+} microdomains exist in the apical pole of secretory cell and presynapse to grant the readily docked secretory vesicles the advantage of exposure to a very brief but extraordinarily

high $\Delta[Ca^{2+}]_i$. The local high $[Ca^{2+}]_{PM}$ is crucial for the vesicles to fuse to the plasma membrane and release their contents. .

To date, the majority of studies on Ca^{2+} signaling in microdomain were carried out in neuronal and muscle cells, both of which are excitory cells. The amplitude and duration of the $[Ca^{2+}]_i$ change at the PM microdomain ($\Delta[Ca^{2+}]_{PM}$) and the size of the microdomain "hot spot" have been characterized (Marsault et al., 1997). However, the mechanisms responsible for maintaining and regulating $[Ca^{2+}]_{PM}$ have remained elusive, mainly because of the difficulties in visualizing Ca^{2+} microdomain due to lack of high resolution optical sectioning methods. The emergence of the Total Internal Reflection Fluorescence Microscopy (TIRFM) imaging provides a solution to the requirement of resolution.

TIRFM has been employed in various studies to assay $[Ca^{2+}]_{PM}$, such as visualization of local "hot spots" of Ca^{2+} elevations in neurons (Navedo et al., 2005), monitoring the fusion of synaptic vesicles (Zenisek et al., 2000), and trafficking of ion channels such as TRP channels (Smyth et al., 2006). However, the properties of $[Ca^{2+}]_{PM}$ and its relationships to the bulk cytosolic Ca^{2+} ($[Ca^{2+}]_{Cyto}$) has not been studied. In present study, I use TIRF microscopy, combined with a low affinity fluorescent Ca^{2+} dye, Fluo-3, to distinguish $[Ca^{2+}]_{PM}$ from $[Ca^{2+}]_{Cyto}$ to study the Ca^{2+} dynamics of these two compartments and how they are differentially regulated.

3.2 Evidence for high $[Ca^{2+}]_{PM}$ in response to supramaximal agonist stimulation

In the first sets of experiments, I measured the increase of $[Ca^{2+}]_{PM}$ under agonist stimulations and verified the feasibility of TIRF in the present studies. Each experiment was individually calibrated, therefore $\Delta[Ca^{2+}]_i$ can be quantified and summarized.

At resting state $[Ca^{2+}]_{PM}$ and $[Ca^{2+}]_{Cyto}$ showed no difference. In regular Ca^{2+} containing media, $[Ca^{2+}]_{PM}$ is 53.5±7.8 nM (n=12) while $[Ca^{2+}]_{Cyto}$ is 51.3±6.1nM (n=12) (number in parenthesis indicates the total number of recording). In Ca^{2+} free media, $[Ca^{2+}]_{PM}$ is 50.6±5.9nM, (n=14), while $[Ca^{2+}]_{Cyto}$ is 50.3±6.8nM (n=14). It appeared that external Ca^{2+} concentration ($[Ca^{2+}]_O$) had no effects on $[Ca^{2+}]_i$ in either compartment at resting state (Fig 3-1B). In the presence of Ca^{2+}, acinar cells were exposed to 1mM of carbachol (Carb), the $[Ca^{2+}]_{PM}$ peak reached 1111.8±225.5nM (n=14) while $[Ca^{2+}]_{Cyto}$ only increases to as high as 419.0±71.0nM (n=14). Thus, $\Delta[Ca^{2+}]_{PM}$ was 2.9-fold larger than $\Delta[Ca^{2+}]_{Cyto}$ at the initial releases. When external Ca^{2+} was removed from bath solution after the Ca^{2+} profiles stabilized, $[Ca^{2+}]_{PM}$ was at a steady state of 197.3±24.1nM (n=11) while $[Ca^{2+}]_{Cyto}$ was 90.4±10.6nM (n=11). Once the $[Ca^{2+}]_i$ came back to basal level, Ca^{2+} was re-added to bath solution.

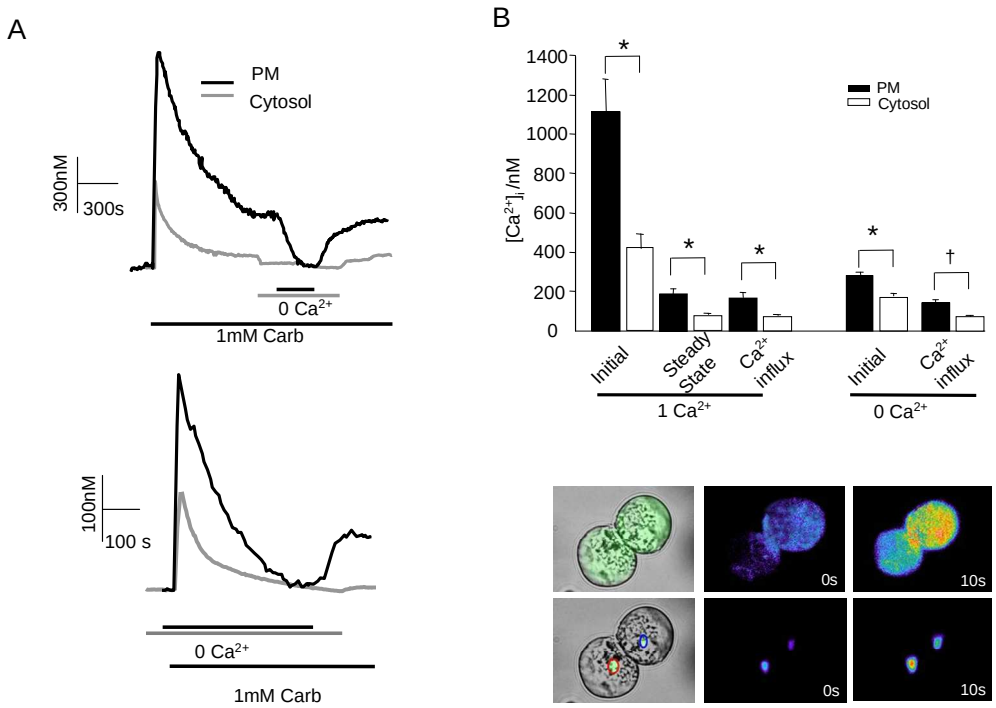

Figure 3-1 $[Ca^{2+}]_{PM}$ had larger initial discharge and influx than $[Ca^{2+}]_{Cyto}$ upon supramaximal carbachol stimulation.

A) Pancreatic acinar cells were stimulated with 1mM carbachol (Carb) in the presence (upper panel) or in the absence (lower panel) of external Ca^{2+}. The magnitude of Ca^{2+} influx was determined by re-addition of Ca^{2+} to the bath solution after $[Ca^{2+}]_i$ stabilized in Ca^{2+}-free environment. The duration of acini exposing to Ca^{2+}-free medium was indicated by bars, 1mM Ca^{2+} was in present otherwise. Representative profiles of Ca^{2+} changes in the near membrane microdomain and in the bulk cytosol were superimposed. B) $\Delta[Ca^{2+}]_i$ was summarized. (* P<0.01 †P<0.05 with indicated number of experiments)

The increase in $[Ca^{2+}]_i$ is attribute to influx-mediated calcium release. The peak of $[Ca^{2+}]_{PM}$ was 185.2±15.1nM (n=10) and peak of $[Ca^{2+}]_{Cyto}$ was 87.3±11.4nM (n=10). Thus, $\Delta[Ca^{2+}]_{PM}$ by influx was nealy 4 folds larger than $\Delta[Ca^{2+}]_{Cyto}$ (Fig 3-1A,1B)

Acinar cells were also subjected to carbachol stimulation in the absence of external Ca^{2+}. This allowed us to separate an initial Ca^{2+} discharge release from the contribution of Ca^{2+} influx depending on external Ca^{2+}. The data showed a 4.8 fold reduction in $\Delta[Ca^{2+}]_{PM}$ (269±12.0nM n=12) and a 2.8 fold reduction in $\Delta[Ca^{2+}]_{Cyto}$ (183.5±10.7nM n=12). After the initial release, $[Ca^{2+}]$ of both compartments went back to resting level due to the exhaustion of the external Ca^{2+} supply. Adding back external Ca^{2+} led to an $[Ca^{2+}]$ increase in microdomain to 155.5±8.3nM (n=7) and in the cytosol to 85.8±7.4 (n=7).

3.3 Agonists evoked $[Ca^{2+}]_{PM}$ oscillations were more sensitive to $[Ca^{2+}]_O$

Low strength of agonists evoke oscillatory releases of Ca^{2+} in pancreatic acinar cells rather than a single robust and long lasting rise. This feature is crucial for acinar cells to exert secretion functions in a prompt and well regulated manner. Dynamics of oscillatory Ca^{2+} spikes convey information on how Ca^{2+} release, re-uptake and exclusion are controlled. In order to understand the mechanisms of the differential regulation of $[Ca^{2+}]_{PM}$ and $[Ca^{2+}]_{Cyto}$ under physiological stimulation, I stimulated acinar cell with 10 pM CCK. After 3-4 oscillatory spikes, external Ca^{2+} was removed. The frequency of oscillations was the same between the near-membrane microdomain and cytosol as averaged from 34 pairs of experiments (Fig 3-2A, 2B). Simultaneous recording of $\Delta[Ca^{2+}]_{PM}$ and $\Delta[Ca^{2+}]_{Cyto}$ confirmed this result (data not shown). Once Ca^{2+} was removed, oscillatory spikes in both compartments declined although in different manners.

In near-membrane microdomain, the frequency of the oscillation is decreased while the amplitude is kept at the same till fully stopped. On the contrary, cytosolic Ca^{2+} oscillation decayed in both amplitude and frequency. Generally, it took longer for cytosolic oscillations to diminish than for near-membrane oscillations. The same trend was observed when oscillations were initiated in Ca^{2+} free medium (Fig 3-2A, lower panel).

Another prominent feature of the dynamics of near-membrane microdomain is that after oscillations were stopped due to lack of Ca^{2+} influx, re-addition of Ca^{2+} back to the bath solution restored it to similar amplitude and frequency (27 out of 34 cells). In contrast, this type of recovery was rare in the bulk cytosol (4 out of 25 cells), only a small sustained influx could be detected (Fig 3-2A).

The above mentioned features were not agonist-specific. As shown in Fig 3-2C, cells were also stimulated with 0.5μM carbachol instead of CCK, oscillations of $[Ca^{2+}]_{PM}$ decayed only in frequency but not in amplitude while $[Ca^{2+}]_{Cyto}$ oscillations decrease in both properties in Ca^{2+} free environment. Regardless whether the oscillations were started in the presence or absence of external Ca^{2+}, near-membrane microdomain can resume oscillation but cytosol cannot.

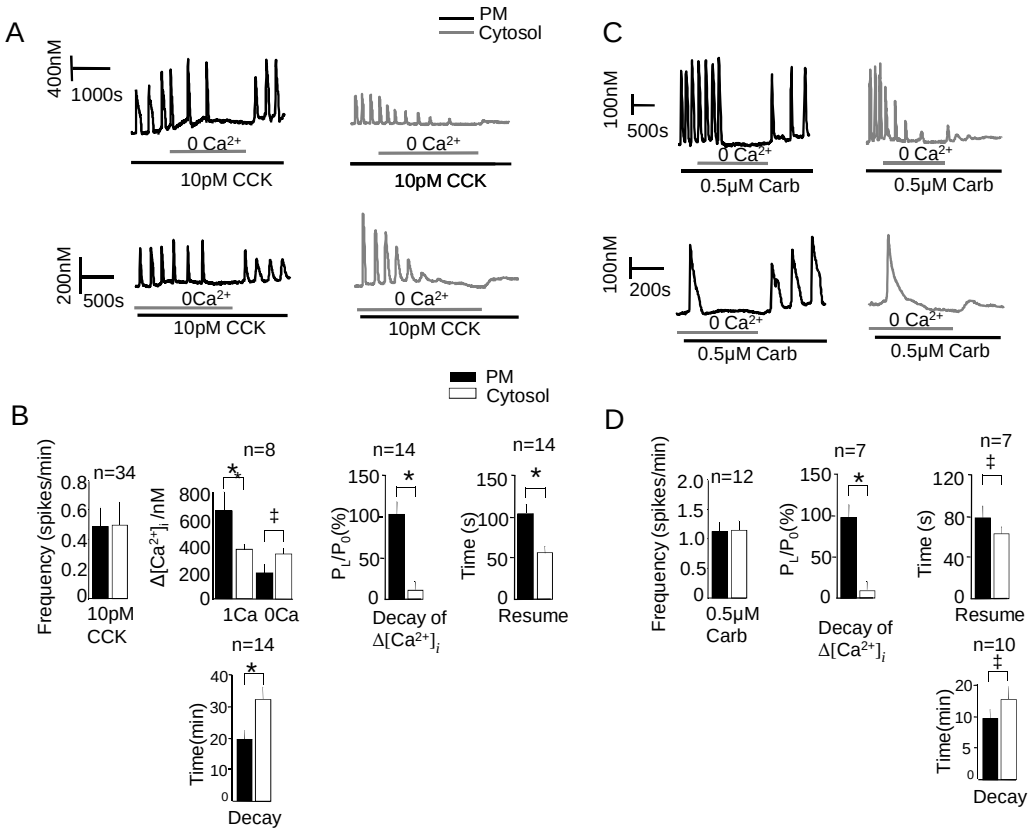

Figure 3-2 Response to low concentration of IP_3-generating agonists and effect of removal-readdition of external Ca^{2+}.

A) Acinar cells were stimulated with 10pM CCK. After three agonist induced $[Ca^{2+}]_i$ spikes in regular bath solution (upper traces), Ca^{2+} was removed until oscillations completely stopped. Then cells were re-exposed to 1mM Ca^{2+} for at least 600s to allow the store reload. Alternatively, cells were first exposed to CCK in Ca^{2+}-free media, 1mM Ca^{2+} was supplemented to the bath solution after oscillations stopped. B) Summary of characterizations of CCK elicited $[Ca^{2+}]_i$ oscillations. C) Acinar cells were treated under conditions as in A) but with 0.5 μM Carb and D) is the quantitative summary of C). (* $P<0.01$, ‡ $P<0.05$ with indicated number of experiments)

3.4 Different effects on microdomain and cytosol Ca^{2+} by inhibition of SERCA

In pancreatic acinar cells, agonist-evoked Ca^{2+} releases start from the apical poles and propagate through the cells like a wave. SERCA pump inhibitors, on the other hand, cause a global $[Ca^{2+}]_i$ elevation by preventing Ca^{2+} uptake into ER. The next question I wanted to address was whether the dynamics of $[Ca^{2+}]_{PM}$ and $[Ca^{2+}]_{Cyto}$ is different if Ca^{2+} release is induced by a SERCA pump inhibitor. As showed in Fig 3-3A, 1 μM of CPA induced oscillation (13 out of 17 cells) in near-membrane microdomains but elicit a long lasting elevation in cytosol (15 out of 15 cells). CCK was able to mobilize only a small amount of Ca^{2+} following the initial release possibly because the store had been partially depleted. On the other hand, if the oscillations were elicited by 10 pM CCK, addition of 1μM CPA stopped oscillations in cytosol as quickly as within one oscillatory cycle. In contrast, the frequency of $[Ca^{2+}]_{PM}$ oscillation was raised by 1μM of CPA. Addition of 10 μM CPA on top of CCK resulted in a robust rise in $[Ca^{2+}]_I$, exhausting oscillations in both compartments (Fig 3-3B).

Low concentration of CPA was capable of inducing $[Ca^{2+}]_{PM}$ oscillation even in Ca^{2+}-free medium and re-addition of external Ca^{2+} led to a greater $\Delta[Ca^{2+}]_{PM}$ than $\Delta[Ca^{2+}]_{Cyto}$ (2.5 fold with 1μM CPA and 4.7 fold with 10μM CPA) (Fig 3-3C).

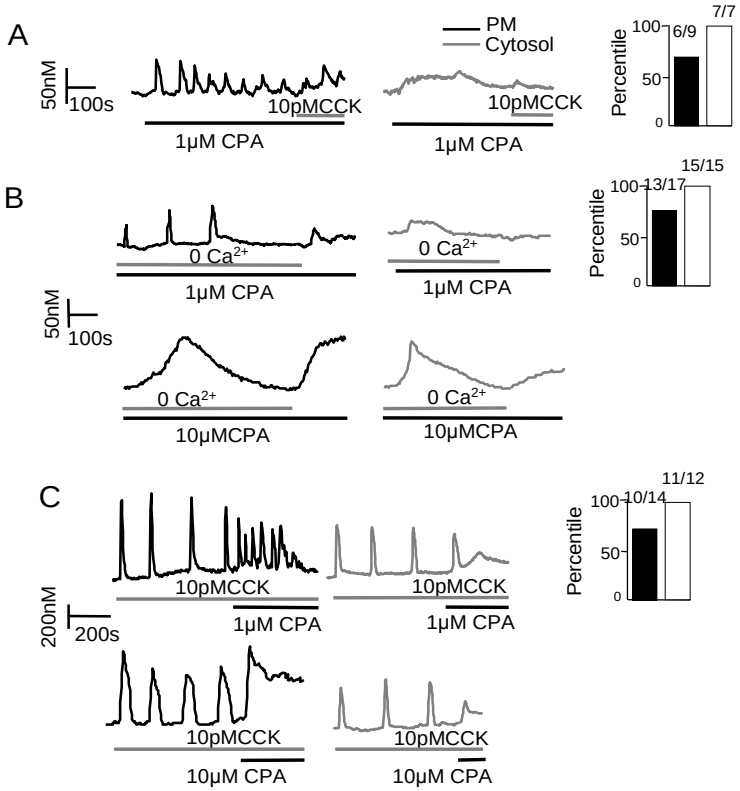

Figure 3-3 $[Ca^{2+}]_{PM}$ and $[Ca^{2+}]_{Cyto}$ respond differently to the inhibition of SERCA pump by CPA.

A) Acinar cells were treated with 1μM CPA followed by 10pM CCK in continuous presence of Ca^{2+}. Low CPA induced $[Ca^{2+}]_{PM}$ oscillations but a sustained rise in $[Ca^{2+}]_{Cyto}$. B) Cells were exposed to CPA first in Ca^{2+} free then in regular Ca^{2+} (1mM) medium. With low [CPA], $\Delta[Ca^{2+}]_{PM}$ oscillated in the absence of external Ca^{2+} while $[Ca^{2+}]_{Cyto}$ only showed a modest transient rise.. High [CPA] resulted in a single robust spike in both compartments. Ca^{2+} influx was more robust in microdomain under both low and high [CPA]. C) Cells were stimulated with 10pM CCK to establish oscillation, then 1μM or 10μM CPA was added to trigger Ca^{2+} discharge from the internal stores. $[Ca^{2+}]_{PM}$ maintained oscillatory transients longer than $[Ca^{2+}]_{Cyto}$ did under 1μM CPA. With 10μM CPA, oscillatory transients of both compartments dissolve equally fast.

3.5 Characterization of ionomycin induced $\Delta[Ca^{2+}]_{Cyto}$ and $\Delta[Ca^{2+}]_{PM}$

The apparent disparity between $[Ca^{2+}]_{Cyto}$ and $[Ca^{2+}]_{PM}$ upon stimulation could be due to different regulation mechanism or different size of the Ca^{2+} reservoir. To distinguish between these two possibilities, I used ionomycin, a Ca^{2+} ionophore, to mobilize Ca^{2+} in both compartments. Low to high concentrations of ionomycin (1-10μM) were used to induce elevation of $[Ca^{2+}]_i$ in the absence of external Ca^{2+}. Representative Ca^{2+} profiles are shown in Fig 3-4A. In the cytosol, as low as 1μM ionomycin induced a Ca^{2+} signal near saturation. $[Ca^{2+}]_{PM}$ transient, despite the fact that it showed larger rise than $\Delta[Ca^{2+}]_{Cyto}$ during the carbarcol treatment, was much lower in amplitude. At 1μM ionomycin, $\Delta[Ca^{2+}]_{PM}$ was nearly half of $\Delta[Ca^{2+}]_{Cyto}$ at peak. Higher ionomycin introduced minor increase in $\Delta[Ca^{2+}]_i$. Surprisingly, with increasing concentration of ionomycin, peak $\Delta[Ca^{2+}]_{Cyto}$ increased as expected while peak $\Delta[Ca^{2+}]_{PM}$ decreased. The difference between $\Delta[Ca^{2+}]_{PM}$ at 1μM and 10μM ionomycin was statistically significant(Fig 3-4B). It is noteworthy that the duration of Ca^{2+} transients of both compartments first increased and then decreased with the increasing concentration of ionomycin. The duration of the Ca^{2+} transient peaked at 2μM ionomycin in the microdomain while the peak concentration for cytosol is 5 μM (Fig 3-4C).

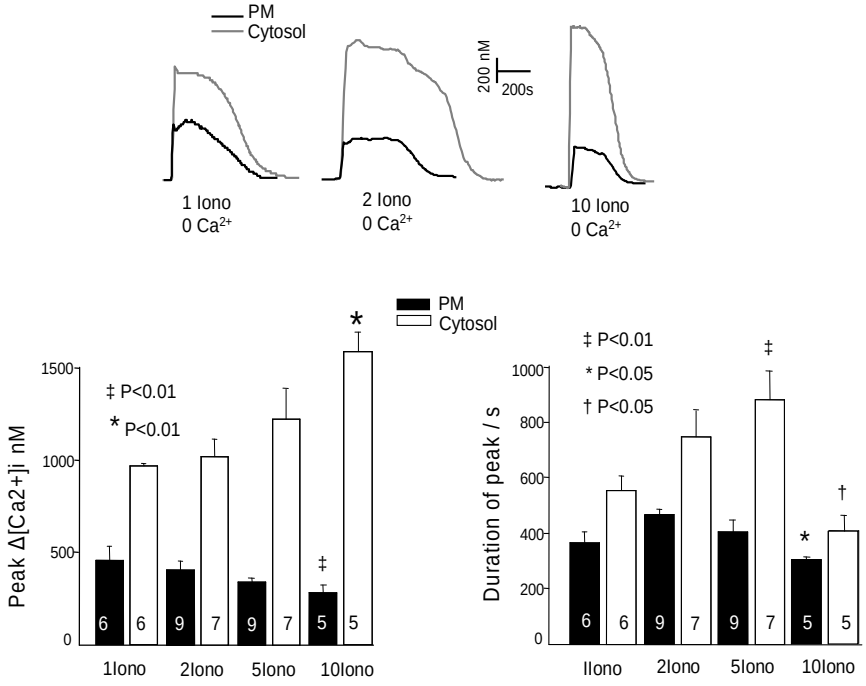

Figure 3-4 Maximal Ca^{2+} release from internal store by ionomycin.

Acini were treated with different concentrations of ionomycin (1-10μM). Amplitude of $\Delta[Ca^{2+}]_i$ and duration of Ca^{2+} releases were summarized. A) Superimposed traces showed contrast between the dynamics of $[Ca^{2+}]_{PM}$ and $[Ca^{2+}]_{Cyto}$. $\Delta[Ca^{2+}]_{PM}$ was less robust and narrower under all circumstances. B) Summary of $\Delta[Ca^{2+}]_i$ and duration.

The area under the profile curve is in proportion to the total Ca^{2+} released during the process. It appeared that ionomycin, at any concentration, was able to mobilize only a much smaller portion of Ca^{2+} for the near membrane microdomain than for the bulk cytosol. This finding is in agreement with the sense of microdomain being a superficial space beneath the plasma membrane. It is not unexpected that it possesses such limited Ca^{2+} storage.

3.6 Discussion

In this study, I have characterized the different regulation of the dynamics of $[Ca^{2+}]_{PM}$ and $[Ca^{2+}]_{Cyto}$. $\Delta[Ca^{2+}]_{PM}$ was larger during agonists evoked Ca^{2+} releases and the subsequent Ca^{2+} influx. Under stimulation by low concentration of agonist, $[Ca^{2+}]_{PM}$ oscillations appeared to be affected by external Ca^{2+} more than $[Ca^{2+}]_{Cyto}$ was. The amplitude of $[Ca^{2+}]_{PM}$ spikes decreased by three folds in Ca^{2+} free medium. On the other hand, microdomain was less sensitive to the stimulation of CPA on top of CCK-induced oscillation. Near-membrane oscillations persisted for longer period than in cytosol under this circumstance. Also, microdomain appeared to be less sensitive to ionomycin treatment. Ionomycin has been routinely used to maximally mobilize internal Ca^{2+}. In near-membrane microdomains, even with 10μM of ionomycin, only a low amplitude and brief transient could be detected. This implied either a store that is less permeable to ionomycin, or an extraordinary efficient mechanism of excluding Ca^{2+} that exists in the microdomain so that Ca^{2+} never builds up during releasing.

In the present study, $[Ca^{2+}]_{Cyto}$ and $[Ca^{2+}]_{PM}$ data were recorded from different acini and all quantitative features were summarized from the average of multiple

measurements. Ideally, it will be best to acquire TIRFM and WFM imaging data simultaneously from the same acinus. Our current setup of TIRFM accommodated semi-simultaneous recording. By combining a secondary light source to excite the wide field fluorescence microscope and using an external motor to control the focus plane from image to image, TIRFM and WFM images can be recorded alternatively. However, interchange between two recording modes caused severe decays in fluorescence intensities due to the high power of exciting beam to achieve fair signals. Thus, I can only use this method to confirm that the CCK-evoked oscillations were of the same frequency in the microdomain as in the bulk cytosol. It was not possible to compare the amplitude of the two measurements in this setting. In the future, it will be very helpful to be able to examine $[Ca^{2+}]_{PM}$ and $[Ca^{2+}]_{Cyto}$ on the same cells, which would allow a direct comparison of Ca^{2+} dynamics between the two compartments.

The differences observed between the two compartments in the study were not as drastic as predicted or previously demonstrated. High $[Ca^{2+}]_{PM}$ microdomains have been observed in various cells, by using Ca^{2+} reporters such as Ca^{2+} activated K^+ current, photolysis of caged Ca^{2+} or membrane-targeted aequorin (Marsault et al., 1997). Although it was reported that $[Ca^{2+}]$ transients can reach the scale of hundreds of micromolar, it is still under debate about how much $[Ca^{2+}]$ is required to elicit exocytosis(Neher, 1998).

My studies showed that upon stimulation, $[Ca^{2+}]_{PM}$ can rise up as high as hundreds of nanomolar to several micromolar concentration, and $[Ca^{2+}]_{PM}$ and $[Ca^{2+}]_{Cyto}$ are the same at resting state. One explanation to this discrepancy is the optical resolution of the microscope method. Although the theoretical resolution of TIRF is approximate

100 nm from the plasma membrane; the actual depth of focal plane would be 200-300nm. That means what I recorded by TIRFM is a mixed signal containing both $[Ca^{2+}]_{PM}$ from near membrane microdomain and $[Ca^{2+}]_{Cyto}$ from the immediate cytosol environment around the near membrane microdomain. Nevertheless, TIRFM detected the unique characteristics of the different regulation of each compartment, which validate the use of TIRF as a suitable method for this type of study.

When studying the microdomain by TIRFM, one should also take into account the location on the cells where the recording was obtained since this may affect both the amplitude and the kinetics of $[Ca^{2+}]_i$. My investigation focused on the $\Delta[Ca^{2+}]_{PM}$ events of the microdomain right under the plasma membrane, which, most likely, is not a globally homogeneous space. It has been showed that in pancreatic acinar cells, agonist induced Ca^{2+} waves always start from the apical pole and propagate through the basal-lateral region. So it is believed that the apical region possesses Ca^{2+} store with higher affinity/sensitivity to IP_3 (Thorn, 1993). Polarize Ca^{2+} signaling in pancreatic acinar cells should be reflected by the Ca^{2+} dynamics in the microdomain too. However, due to the architecture of the pancreatic acini, most of the acinar cells attached to coverslips by basal-lateral membrane. This means that in some experiments I could be recording away from the true initial site of Ca^{2+} release, causing the reading to be lower than reported elsewhere. Nonetheless this drawback should not affect the measurements on $[Ca^{2+}]_{PM}$ oscillations pattern.

Only $[Ca^{2+}]_{PM}$, but not $[Ca^{2+}]_{Cyto}$, demonstrated recovery of oscillations after cycles of removing and replenishing external Ca^{2+}, despite of fact that it took microdomain longer to see increase in $[Ca^{2+}]_i$. This unique feature may reflect the need

for the cell to be ready for repeating exocytosis. Microdomain needs to be quickly refilled once the Ca^{2+} store is depleted, which may be the result of prolonged stimulation, to resume oscillatory Ca^{2+} spikes while cytosol is still in the process of reloading. For the same reason, the amplitude of oscillatory spikes are kept unchanged till the last one during Ca^{2+} free incubation, thus the Ca^{2+} activated exocytosis events will be minimally affected before microdomain run out of Ca^{2+} in the store.

In summary, I have demonstrated that $[Ca^{2+}]_{PM}$ and $[Ca^{2+}]_{Cyto}$ are differently regulated. $[Ca^{2+}]_{PM}$ is more sensitive to $[Ca^{2+}]_{O}$ following stimulations but less sensitive to passive store depletion by CPA or global discharge by ionomycin. These findings provide evidence of the compartmentalization of near membrane microdomain and emphasize its roles in cellular functions in pancreatic acinar cells. Meanwhile, TIRF was verified as a feasible way to investigate $[Ca^{2+}]_{PM}$ in exocrine cells in addition to other established methodologies.

Chapter 4 Ca^{2+}-Induced Ca^{2+} Release in Parotid Acinar Cells is Mediated by the Activation of SOC and RyR

4.1 Background

Ca^{2+} induced Ca^{2+} release (CICR) as a mechanism that links excitation and contraction in muscle cells is well established (Fill and Copello, 2002). However, the regulation of this type of Ca^{2+} release in non-excitable cells remains to be clarified.

CICR is mediated by the ryanodine receptors (RyRs). The cell specific expression of three RyR isoforms was reviewed in Chapter One. The primary activator of RyRs in muscle cells is Ca^{2+}. However, the stimulant to trigger Ca^{2+} flux is cell specific. In skeletal muscle RyR1 directly interacts with the voltage-regulated L-type Ca^{2+} channel. The L-type channel functions as a voltage sensor that senses the membrane depolarization to undergo a conformational change and activate RyR1. The initial Ca^{2+} released through RyR1 further activates RyR1, leading to the explosive Ca^{2+} release that mediates muscle contraction (Fill and Copello, 2002; Franzini-Armstrong and Protasi, 1997). By contrast, in cardiac muscle the L-type channel is not directly coupled to RyR2. Rather, the L-type channel is localized adjacent to RyR2. Membrane depolarization results in activation of the L-type Ca^{2+} channel and Ca^{2+} influx. The incoming Ca^{2+} serves as the trigger to activate RyR2 in the cardiac SR and cause the explosive Ca^{2+} release and muscle contraction (Bers, 2002; Fill and Copello, 2002).

I chose the parotid acinar cells to study the regulation of CICR for two reasons. First, there is evidence for expression and function of RyRs in these cells and experimental findings suggesting activation of Ca^{2+} release by a RyR ligand cADPR.

Second, cADPR is capable of releasing the entire agonist-mobilizable Ca^{2+} store in parotid acinar cells. These results are notably different from those reported in pancreatic acinar cells by several groups, in which cADPR was able to mobilize only a small fraction of the agonist-mobilizable store (Leite et al., 2002; Sneyd et al., 2003; Straub et al., 2000; Thorn et al., 1994). All current models to explain the role of RyRs in non-muscle cells depict them to be sensitized by cADPR to Ca^{2+}, which is released from the IP_3-sensitive Ca^{2+} pool. My work examined the activation mechanism and source of triggering Ca^{2+} in the CICR in parotid acinar cell.

4.2 Identification of CICR in parotid

To study the Ca^{2+} dynamics, I used small clusters of parotid acinar cells to measure the whole cell $[Ca^{2+}]_i$ change, using Fura 2 as indicator. When stimulated with agonist carbachol, a unique pattern of Ca^{2+} dynamics was observed in the presence of 1 mM of extracellular calcium. Agonist like carbachol usually induces a spike of initial Ca^{2+} increase in parotid acinar cell (Fig 4-1A, indicated by arrow). In the presence of agonist and 1mM extracellular Ca^{2+}, $[Ca^{2+}]_i$ went up again and formed a large and sustained $[Ca^{2+}]_i$ increase before it returned to base line (Fig 4-1B).

The secondary Ca^{2+} release relies on both agonist-activated receptor and the presence of extracellular Ca^{2+}. Removal of either caused $[Ca^{2+}]_i$ to go back to baseline. Re-addition of Ca^{2+} to the medium in the presence of carbachol induced new $[Ca^{2+}]_i$ increase that is comparable in magnitude to the original peak. The characteristic of such kind of calcium dynamics upon agonist stimulation suggests Ca^{2+}-induced Ca^{2+} release (CICR). Studies performed by my colleague showed that cyclic ADP ribose (cADPR),

an endogenous activator of RyRs, activated the Ca^{2+}-activated Cl^- current in parotid acinar cells. Since such current is an indicator of the changes in $[Ca^{2+}]_i$, the result confirmed that cADPR is able to mobilize the internal Ca^{2+} stores, most likely through RyRs. Most of the IP_3-dependent stores can also be activated by cADPR because addition of maximum carbachol on top of 10 μM cADPR only lead to minimum increment in $[Ca^{2+}]_i$ (Fig 4-1C, D).

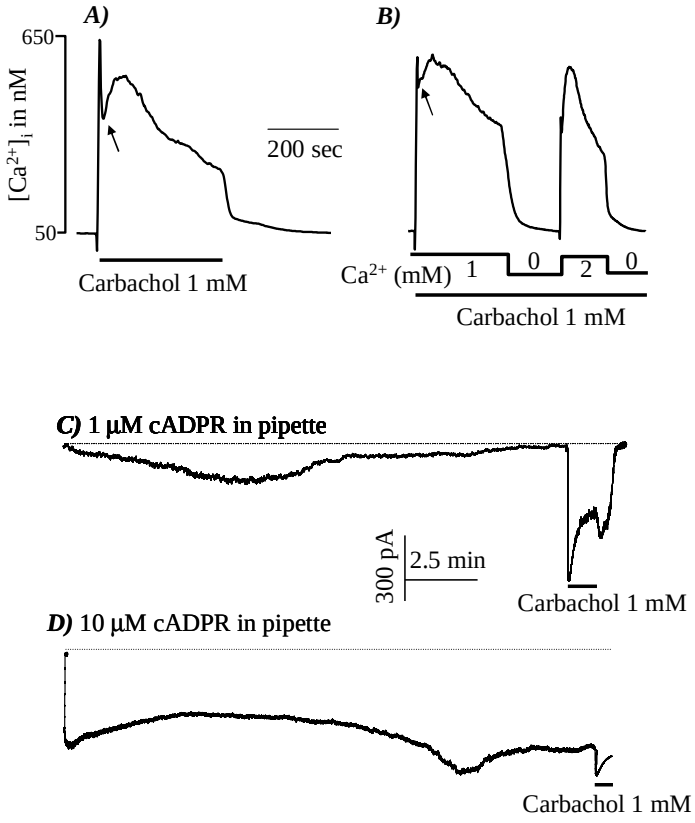

Figure 4-1 Effect of carbachol on $[Ca^{2+}]_i$ and Ca^{2+} release by cADPR.

Small acinar clusters (5-8 cells) loaded with Fura2 were used to measure $[Ca^{2+}]_i$ (A, B). As indicated by the bars, the cells were stimulated with 1 mM carbachol and perfused with solutions containing 0, 1 or 2 mM $CaCl_2$. Single parotid acinar cells (C-D) were used to measure the Ca^{2+}-activated Cl^- current. Pipette solution contained 1 (C) or 10 μM (D) cADPR. Where indicated by the bars, the cells were stimulated with 1 mM carbachol.

To prove that the observation is indeed CICR, it is necessary to distinguish between the contribution of Ca^{2+} influx and Ca^{2+} release to a typical Ca^{2+} peak. When parotid cells were stimulated with 1 mM carbachol in the absence of extracellular Ca^{2+}, $[Ca^{2+}]_i$ only increased from 49 ± 6 nM to 186 ± 21 nM (n=17) for a very brief period of time before returning to base line (Fig. 4-2A). This is in sharp contrast to the robust increase of $[Ca^{2+}]_i$ as in Fig. 4-1A. The area under the curve, which is in proportion to the total amount of Ca^{2+} entering the cytosol, was reduced by nearly 90%. This suggests that agonist stimulation by itself can only mobilize a fraction of the Ca^{2+} store in the parotid acinar cells. The other components constituting a Ca^{2+} release peak as seen in Fig 4-1A may include Ca^{2+} influx following the initial release and CICR by the influx. Re-addition of Ca^{2+} to the medium caused a two-phase increase of $[Ca^{2+}]_i$. A slow initial phase was observed followed by a more explosive second phase. The turning point is indicated by arrows in Fig 4-2A. When 7.5 mM Ca^{2+} was added to the perfusion buffer, an explosive release was observed immediately. $[Ca^{2+}]_i$ increased to 435 ± 39 nM (n > 50 acini). The magnitude of $[Ca^{2+}]_i$ change under this condition was about three times of that induced by the agonist in Ca^{2+}-free medium.

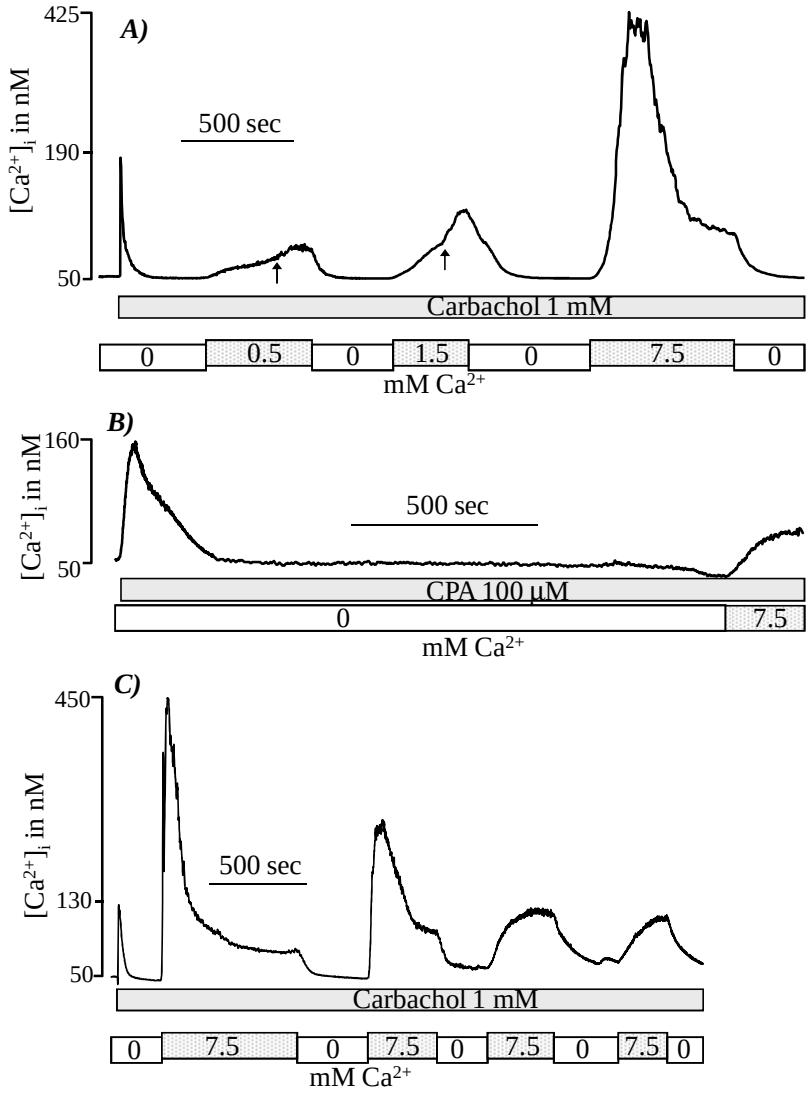

Figure 4-2 Effect of external Ca^{2+} on $[Ca^{2+}]_i$.

Acini perfused with Ca^{2+}-free medium were stimulated with 1 mM carbachol (A, C) and were then perfused alternately with media containing 0.5, 1.5, 7.5 or 0 mM Ca^{2+} (A) or alternately with media containing 7.5 or 0 mM Ca^{2+} (C). The acini in (B) were treated with 100 µM CPA in Ca^{2+}-free medium for about 20 min and then exposed to a medium containing 100 µM CPA and 7.5 mM Ca^{2+}.

Prolonged treatment of cells by cyclopiazonic acid (CPA), an inhibitor of SERCA pump, may have completely depleted the Ca^{2+} stores, therefore eliminating its contribution to the $[Ca^{2+}]_i$ increase. Addition of 7.5 mM Ca^{2+} to the incubation medium after depletion of Ca^{2+} stores in Ca^{2+} free medium caused $[Ca^{2+}]_i$ to slowly increase to and stabilize at 138 ± 11 nM (n=5) above resting level (Fig 4-2B). This signal likely represents only Ca^{2+} influx across the plasma membrane without Ca^{2+} release from the internal stores. The explosive $[Ca^{2+}]_i$ increase as seen in Fig. 4-1B and 4-2A differs in at least two ways from the $[Ca^{2+}]_i$ by influx: quicker in responsiveness and more robust in magnitude at the peak of the signal.

Most parotid acinar cells I have tested were capable of multiple explosive releases when exposed to media containing alternating 0 and 7.5 mM Ca^{2+} in the constant presence of 1 mM carbachol. As shown in Fig. 4-2C, addition of 7.5 mM Ca^{2+} resulted in two (up to three in some other cells) robust Ca^{2+} releases followed by a weaker Ca^{2+} peak. The fourth addition of 7.5 mM Ca^{2+} only slowly increased $[Ca^{2+}]_i$ to an average of 142 ± 16 nM (n=8), similar to the signal seen in Fig.4-2B. All the experimental evidences suggested that the explosive Ca^{2+} peaks following high external Ca^{2+} were rapid and robust releases from the internal stores, and this secondary release is dependent on Ca^{2+} influx across the plasma membrane. In another word, Ca^{2+}-induced Ca^{2+} release (CICR) exists in the parotid acinar cells.

4.3 Minimal store depletion is sufficient to induce CICR

Since Ca^{2+}-induced Ca^{2+} release had never been described in parotid acinar cells, I proceeded to further explore the regulatory mechanisms underlying this phenomenon. I

examined the relationship between the extent of cell stimulation and the Ca^{2+} dynamics including both the mobilization of the internal Ca^{2+} stores and the secondary explosive $[Ca^{2+}]_i$ increase induced by 7.5 mM external Ca^{2+}.

A series of different dilutions of carbachol was used to stimulate acinar cells in Ca^{2+} free medium for two minutes to activate acini. 7.5 mM Ca^{2+} was then added to the medium in the continuous presence of carbachol. Data showed that high external Ca^{2+} induced explosive Ca^{2+} release when acini were treated with as low as 0.5 μM carbachol (Fig. 4-3A). 7.5 mM external Ca^{2+} was able to evoked explosive Ca^{2+} release in 1 of 9, 7 of 13 and 25 of 25 experiments, when acini were treated with 0.1, 0.5 and 1.5 μM carbachol respectively. Although 0.5 μM Ca^{2+} did not evoke significant initial $[Ca^{2+}]_i$ increase, it appeared to potentiate the signaling pathway of Ca^{2+} influx and/or Ca^{2+} release.

Next, I wanted to understand whether depletion of internal stores alone or stimulation alone is sufficient to elicit CICR. I used low concentration of CPA to partially deplete internal Ca^{2+} stores. Parotid acinar cells were first treated with 1 μM CPA in Ca^{2+} free medium for various period of time, ranging from 2.5 to 10 min. Next 7.5 mM Ca^{2+} was added to activate Ca^{2+} influx. As shown in Fig. 4-3B, when treated for longer than 5 min, addition of high external Ca^{2+} induced $[Ca^{2+}]_i$ increase. The magnitudes of $[Ca^{2+}]_i$ increase were indeed proportional to the length of the treatment of CPA proceeding the addition of 7.5 mM Ca^{2+}. 7.5 min and longer treatments of 1 μM CPA were sufficient to evoke a robust Ca^{2+} release (Fig. 4-3B).

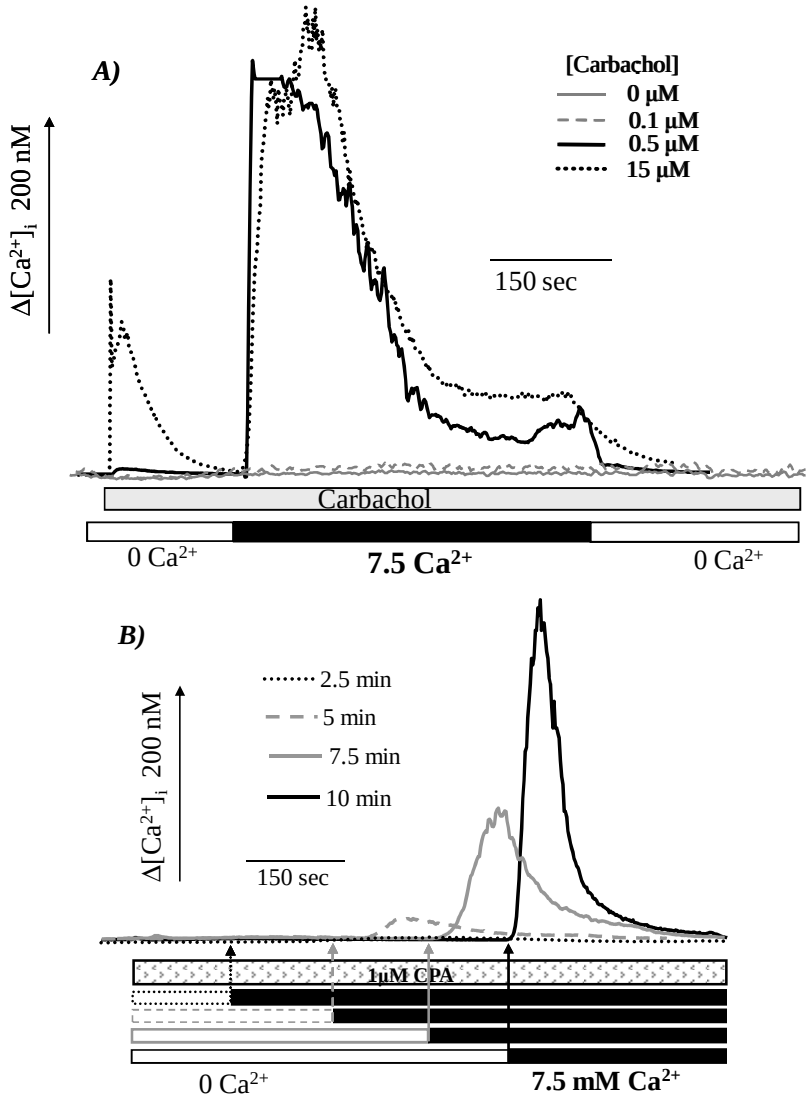

Figure 4-3 Ca^{2+} store depletion and activation of CICR.

(A) Acini incubated in Ca^{2+}-free medium were stimulated with 0 (control, solid gray trace), 0.1 (dashed gray trace), 0.5 (solid black trace) or 15 µM carbachol (dotted black trace) for 2.5 min before exposure to media containing the same carbachol concentration and 7.5 mM Ca^{2+}. (B) The cells were incubated in Ca^{2+}-free medium containing 1 µM CPA for 2.5 (dotted bar), 5 (dashed gray bar), 7.5 (solid gray bar) or 10 min (solid black bar) before addition of 7.5 mM Ca^{2+} to media (filled black bars in each experiment).

Results presented in Fig. 4-3 suggested that minimal depletion of internal stores, instead of agonist stimulation, is sufficient to induce explosive $[Ca^{2+}]_i$ increase. In addition, the data also implicated that the extent of store depletion is a determinant of such signal. In order to assess the extents of depletion necessary to activate CICR, I used a series dilution of CPA ranging from 1 to 100 μM in Ca^{2+}-free medium to sensitize the cells before treating them with 7.5 mM Ca^{2+} and CPA for a prolonged period of time (15 min). Treatment of acini with 2.5 μM and higher concentration of CPA for 2 min was sufficient to induce CICR, similar to the effect of charbacol (n=45 acini) (Fig. 4-4A). In contrast to the massive $[Ca^{2+}]_i$ increase following 7.5 mM Ca^{2+} , CPA stimulation at concentration as high as 100 μM only resulted in a small increase of $[Ca^{2+}]_i$.

Using 2.5, 10 and 100 μM CPA, 3 effective concentrations as determined in Fig. 4-4A, I measured the amount of Ca^{2+} that was mobilized by CPA alone, 100 μM CPA or 1 mM carbachol combined in either 0 Ca^{2+} or 7.5 mM Ca^{2+}. As measured by the area under the curve, Ca^{2+} mobilized by CPA in 0 Ca^{2+} was less than 5% of the total mobilizable stores in Ca^{2+} free media. It constituted even a smaller portion of the total internal stores, which presumably can be fully discharged by 100 μM CPA and 1 mM carbachol in the presence of 7.5 mM external Ca^{2+}(Fig. 4-4B).

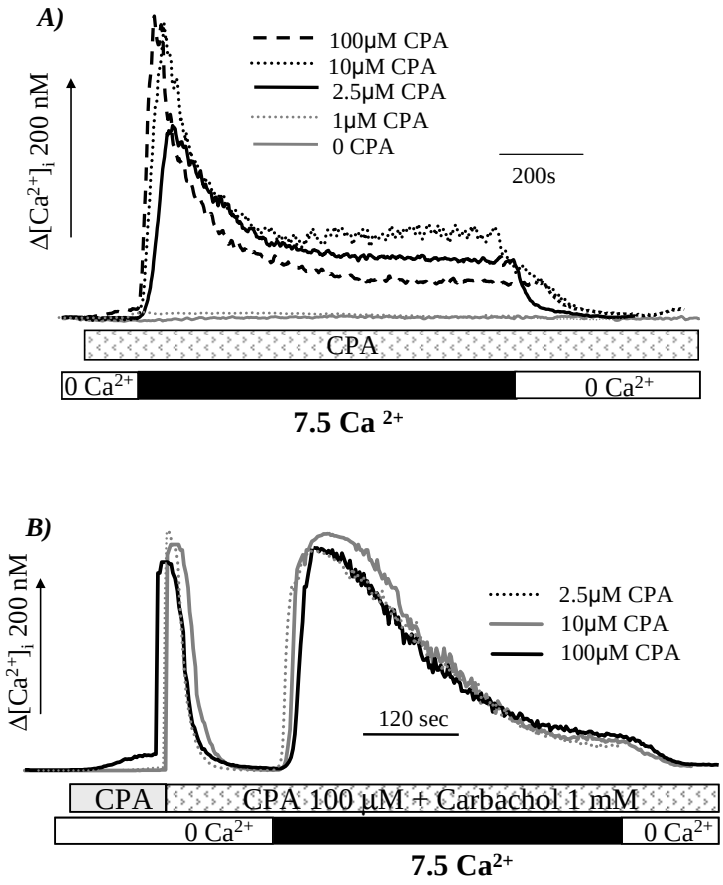

Figure 4-4 Relationship between store depletion by CPA and CICR.

(A) Acini incubated in Ca^{2+}-free medium were treated for 2 min with 0 (control, solid gray trace), 1(dotted gray trace), 2.5 (solid black trace), 10 (dotted black trace) or 100 μM CPA (dashed black trace) before exposure to media containing 7.5 mM Ca^{2+} and then to Ca^{2+}-free media. To estimate extent of store depletion, in (B) acini in Ca^{2+}-free media were treated for 2 min with 2.5 (dotted black trace), 10 (solid gray trace) or 100 μM CPA (solid black trace) before exposure to Ca^{2+}-free media containing 100 μM CPA and 1 mM carbachol. After $[Ca^{2+}]_i$ returned to basal levels the acini were exposed to media containing 7.5 and then 0 mM Ca^{2+}.

4.4 CICR in parotid acini is mainly mediated by RyR

There are two major Ca^{2+} channels in the endoplasmic reticulum membrane: IP_3Rs and RyRs. Both have been demonstrated to be regulated by Ca^{2+}. To determine which one is responsible for the explosive Ca^{2+} release observed in the previous experiments, I used specific blockers against each channel to define their roles in the pathway.

Caffeine blocks IP_3 receptors activation and inhibits the downstream steps of the signaling without affecting cell stimulation and stores depletion. If cells were subjected to caffeine treatment to block IP_3R and store depletion before carbachol, no CICR was observed. By contrast, removal of caffeine reversed the inhibition of CICR. Given long enough recovery time, CICR would resume (Fig, 4-5A).

If caffeine was added after initial stimulation, it was not able to completely inhibit CICR. However, it did slow the rate of Ca^{2+} release. Ca^{2+} entered cytosol in a progressive manner instead of explosive entry (Fig. 4-5B). Caffeine did not affect CPA induced CICR (Fig. 4-5C). These results suggest that the release was through RyR but not through IP_3R.

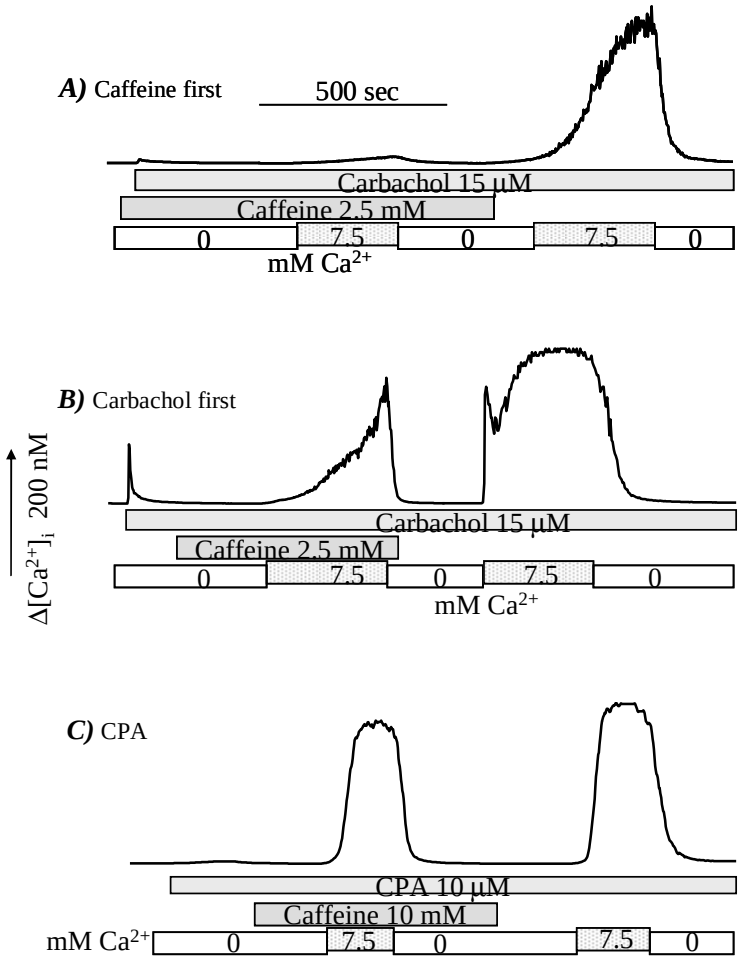

Figure 4-5 CICR does not require active IP_3Rs.

Acini in Ca^{2+}-free medium were incubated with 2.5 mM caffeine before (A) or after (B) stimulation with 15 μM carbachol and then alternately exposed to Ca^{2+}-free media and media containing 7.5 mM Ca^{2+}. Where indicated, caffeine was removed from the perfusion solutions. In (C) acini were incubated with 10 μM CPA for 2 min before treated with 10 mM caffeine in media containing 0 or 7.5 mM Ca^{2+}, as indicated.

4.5 CICR takes place away from plasma membrane

The activity of the Ca^{2+}-activated K^+ channel was measured as an indicator of $[Ca^{2+}]_i$ near the plasma membrane. In preliminary experiments, my colleague and I found no K^+ channel activity when cells were treated with 10 μM CPA in Ca^{2+}-free medium. Addition of 7.5 mM external Ca^{2+} induced a rapid $[Ca^{2+}]_i$ increase but to an unexpected low level compared with the explosive $[Ca^{2+}]_i$ increase measured by fluorescence signals. To explain the discrepancy, I proposed that Ca^{2+} release by CICR is slower and takes place away from the plasma membrane therefore not able to activate K^+ channels as effectively as the initial Ca^{2+} release by agonists.

To further test this theory, we measured Ca^{2+}-activated K^+ current in carbachol stimulated single parotid acinar cells. As shown in Fig. 4-6A, cells were first stimulated with 2.5 μM or 1 mM carbachol in the absence of Ca^{2+} followed by addition of 7.5 mM external Ca^{2+}. In both experiments, 7.5 mM Ca^{2+} induced a K^+ current much weaker compared with the current activated by initial Ca^{2+} release.

Fig. 4-6B showed sample images of changes of $[Ca^{2+}]_i$ in a single parotid acinar cell after carbachol stimulation or after addition of 7.5 mM Ca^{2+}. Carbachol first evoked a typical luminal-to-basal-lateral Ca^{2+} wave in Ca^{2+}-free medium, which reached maximal $[Ca^{2+}]_i$ increase within 0.78s of stimulation. 7.5 mM Ca^{2+} also evoked $[Ca^{2+}]_i$ increase starting from the luminal side. However, it took the cell 2.35 seconds to achieve maximal $[Ca^{2+}]_i$ increase by 7.5 mM Ca^{2+} as evidenced by traces a and b in Fig. 4-7B , although the magnitude of $[Ca^{2+}]_i$ increase was larger . In addition, $[Ca^{2+}]_i$ around the whole basal-lateral region began to increase shortly after addition of 7.5 mM Ca^{2+} and after the increase in luminal pole. Lacking of a luminal-to-basal propagating pattern

implies underlying mechanisms different from the agonist-evoked initial Ca^{2+} release. Even at the apical pole, $[Ca^{2+}]_i$ increase occurred at a slower rate in the case of CICR, as demonstrated by super imposing two apical $[Ca^{2+}]_i$ increases. CICR occurring in regions with less density of IP_3Rs is consistent with results of Fig. 4-5: RyRs, not IP_3Rs, play major roles in the activation of CICR. The more robust $[Ca^{2+}]_i$ increase by 1 mM carbachol is due to more Ca^{2+} released by higher agonist, which compensates for the diffuse distance.

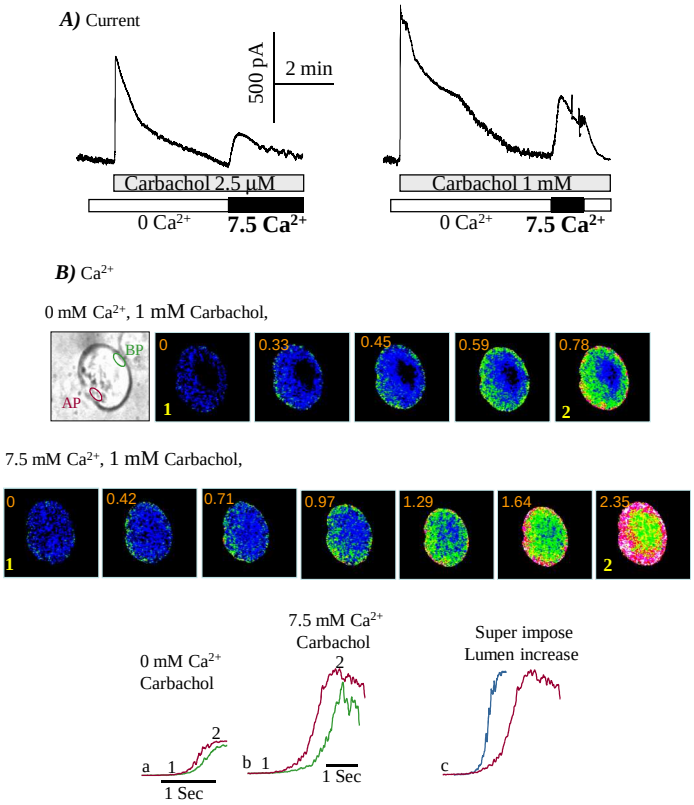

Figure 4-6 Ca^{2+}-activated K^+ current and $[Ca^{2+}]_i$ in single parotid acinar cell.

(A) single parotid acinar cells in Ca^{2+}-free medium were stimulated with 2.5 µM (left trace) or 1 mM carbachol (right trace). After return of the outward current to baseline the external Ca^{2+} was increased to 7.5 mM. In (B) a single cell loaded with fura2 was used to monitor $[Ca^{2+}]_i$. The cell was first incubated in Ca^{2+}-free media and stimulated with 1 mM carbachol (upper images). After return of $[Ca^{2+}]_i$ to baseline the cell was exposed to media containing 1 mM carbachol and 7.5 mM Ca^{2+} (lower images). Images recorded at selective time point during the experiment are shown. The first and last images of each sequence are marked in yellow 1 and 2 and the time of their acquisition is marked at the traces. The first upper image shows the bright field image. The traces in (a, b) show the relative increase of fluorescence at the apical (brown) and basal (green) poles. In (c) the trace of $[Ca^{2+}]_i$ increase at the apical pole due to carbachol stimulation (blue) was scaled up and superimposed with the trace of $[Ca^{2+}]_i$ increase due to addition of 7.5 Ca^{2+} to illustrate the different rates of Ca^{2+} increase. Both traces are drawn at the same time scale.

4.6 Ca^{2+} triggering CICR enters the cell through SOC

It is evident from the previous observations that CICR depends on both depletion of stores and presence of extracellular high Ca^{2+}. The extracellular Ca^{2+} usually enters the cell as influx. However, it is impossible to separate Ca^{2+} influx and Ca^{2+} release spatially and temporally, so the magnitude of Ca^{2+} influx had to be measured indirectly. Mn^{2+} influx is an ideal alternative of measuring Ca^{2+} influx. Most store operated Ca^{2+} channels are of low selectivity and also conduct divalent ions including Mn^{2+}. Moreover, Mn^{2+} is not a substrate to either SERCA pump or PMCA pump, therefore should there be any Mn^{2+} influx following the store depletion, it will faithfully report the activation of Ca^{2+} channels in the membrane.

Treatment of 2.5 μM CPA and 0.5 μM carbachol induced only a slight increase in the rate of Mn^{2+} influx. This is also the concentration of agents that cause minimal cell activation and store depletion. By contrast, treatment with 25 μM CPA and 1 mM carbachol resulted in a drastic increase in the conductance of Ca^{2+} channels. This result demonstrated that CICR is activated through selective activation of Ca^{2+} influx (Fig 4-7)

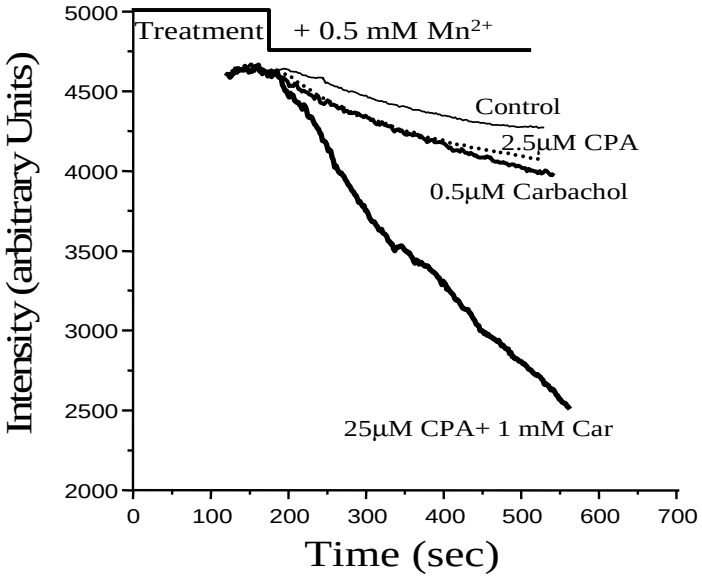

Figure 4-7 Measurement of Mn^{2+} influx.

Acini in Ca^{2+}-free medium were incubated for 2.5 min with 0 (Control), 2.5 μM CPA, 0.5 μM carbachol or 25 μM CPA and 1 mM carbachol, as indicated next to each trace, before exposure to Ca^{2+}-free medium containing the same agonists and 0.5 mM Mn^{2+} to measure Mn^{2+} influx. The first derivatives of the slops were used to obtain the rate of Mn^{2+} influx.

SOCs had been shown to mediate Ca^{2+} conductance upon store depletion in several cell types. Acinar cells were not yet been studied. Here I used two well characterized SOC blockers, SKF96365 and 2-APB. Acini were treated with 10 μM CPA for 2 min in Ca^{2+} free media before addition of 20 or 40 μM SKF96365/2-APB. Administration of SKF96365/2-APB continued until 5 min following 7.5 mM external Ca^{2+}. 20 μM SKF96365/2-APB partially inhibit SOC therefore CICR was reduced in magnitude while 40 μM completely diminish CICR. Inhibition posed by both blockers was reversible, as CICR was restored to a level comparable to control upon removal of the blockers (Fig. 4-8A, B).

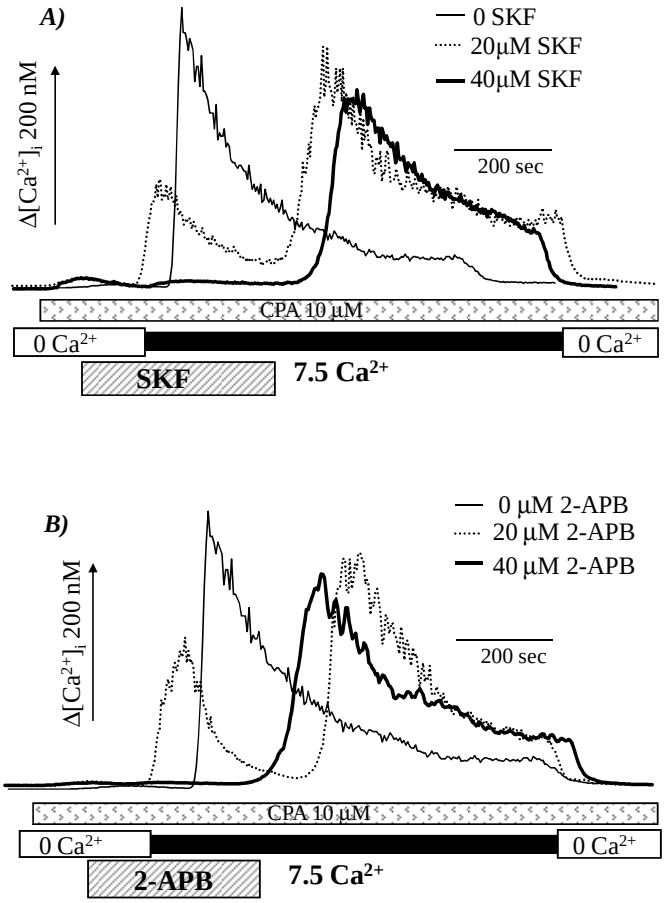

Figure 4-8 Inhibition of Ca^{2+} influx inhibits CICR.

Acini in Ca^{2+}-free medium were treated with 10 μM CPA to activate SOCs and then incubated with 0 (A, B, control, thin solid trace), 20 μM SKF96365 (A, dotted trace), 40 μM SKF96365 (A, thick solid trace), 20 μM 2APB (B, dotted trace) or 40 μM 2APB (B, thick solid trace) before addition of 7.5 mM Ca^{2+} to the incubation media. Blockers were then washed by perfusing the acini with media containing CPA and 7.5 Ca^{2+}.

This study demonstrates CICR in the non-excitable parotid acinar cells, which resembles the mechanism described in cardiac myocytes. Partial depletion of internal Ca^{2+} stores leads to a minimal activation of Ca^{2+} influx. Ca^{2+} influx through this pathway results in an explosive mobilization of Ca^{2+} from the majority of the stores by CICR. Thus, stimulation of parotid acinar cells in Ca^{2+}-free medium with 0.5 μM carbachol releases ~5% of the Ca^{2+} mobilizable by 1 mM carbachol. Addition of external Ca^{2+} induced the same Ca^{2+} release observed in maximally stimulated cells. Similar results were obtained by a short treatment with 2.5–10 μM CPA. The Ca^{2+} release induced by the addition of external Ca^{2+} was largely independent of IP_3Rs because it was reduced by only ~30% by the inhibition of the inositol 1,4,5-trisphosphate receptors with caffeine or heparin. Measurements of Ca^{2+}-activated outward current and $[Ca^{2+}]_i$ suggested that most CICR triggered by Ca^{2+} influx occurred away from the plasma membrane. Measurement of the response to various concentrations of CPA revealed that Ca^{2+} influx that regulates CICR is associated with a selective portion of the internal Ca^{2+} store. The minimal activation of Ca^{2+} influx by partial store depletion was confirmed by the measurement of Mn^{2+} influx. Inhibition of Ca^{2+} influx with SKF96365 or 2-APB prevented activation of CICR observed on addition of external Ca^{2+}. These findings provide evidence for activation of CICR by Ca^{2+} influx in non-excitable cells, demonstrate a previously unrecognized role for Ca^{2+} influx in triggering CICR; and indicate that CICR in non-excitable cells resembles CICR in cardiac myocytes with the exception that in cardiac cells Ca^{2+} influx is mediated by voltage-regulated Ca^{2+} channels whereas in non-excitable cells Ca^{2+} influx is mediated by SOCs.

Chapter 5 Integrity of Microdomains is Essential to Ca^{2+} Regulation

5.1 Background

The roles of ER in orchestrating Ca^{2+} signaling dynamics has been elaborated in Chapter One. An equally important cellular function of ER is its involvement in post-translational processing of protein. In eukaryotes, ER hosts a large variety of enzymes and chaperones that facilitate newly synthesized polypeptide to go through enzymatic modifications and adopt correct folding before achieve their mature conformation. An elaborate quality control mechanism in ER inspects the newly synthesized proteins, which are also referred to as ER client proteins, allowing only the correctly folded proteins to exit ER while misfolded proteins to be degraded (Kleizen and Braakman, 2004; Kostova and Wolf, 2003).

Perturbed modification and folding of client proteins causes ER stress and severe ER stress ultimately results in cell destruction (Aridor and Balch, 1999). To prevent cell death, a mechanism called unfolded protein response (UPR) has evolved to combat ER stress. The UPR pathway is activated by misfolded protein. UPR attenuates ER stress in two ways: by increasing expression of gene involved in the processing of protein folding to speed up the handling of client proteins and by down regulation of new protein synthesis to alleviate the load of client proteins in ER. When a crucial component of UPR pathway is mutated or deleted from cell, it is often observed that misfolded proteins would accumulate in the lumen of ER and cause ER stress. Secretory cells, such as endocrine and exocrine cells, that actively synthesize proteins, and muscle cells that experience large volume of

Ca^{2+} transportation in and out of ER, are particularly susceptible to ER stress(Zhang et al., 2002).

PERK (interferon-inducible RNA-dependent protein kinase-like ER kinase) is a ubiquitously expressed ER residing protein kinase that is a critical component of the UPR pathway. Its N terminus possesses an ER-lumenal sensor domain that can be activated by overload of client proteins. PERK phosphorylates eukaryotic initiation factor eIF2α that in turn inhibits protein translation and attenuates the work load of UPR machinery; hence increases the chance of cellular survival (Harding et al., 2000; Harding et al., 1999; Wu et al., 2002).

PERK is highly expressed in mouse pancreas. PERK-/- mouse experience increased cell death in its pancreas, resulting in diabetes mellitus and exocrine pancreatic insufficiency (Harding et al., 2001). Interestingly, ER in PERK-/- pancreatic acinar cells is often distended and fragmented (Harding et al., 2001). Since the functions of micro domain are highly depended on the integrity of the whole complex, an interesting question arises whether the morphological abnormalities of ER in PERK-/- cells also impair its function as a crucial regulator of Ca^{2+} signaling. In this part of study, I used pancreatic and parotid acinar cells and smooth muscle cells to compare Ca^{2+} dynamics in PERK-/- mouse with wild type.

5.2 Ca^{2+} release is slower in PERK-/- cell

I first measured general Ca^{2+} dynamics in PERK-/- pancreatic acini. Cells were stimulated with 1 mM carbachol to activate the muscarinic receptor mediated Ca^{2+} release from the internal stores. 10 μM atropine was used to terminate the stimulation and allow

the internal stores to reload. The extent of reloading was assessed by re-stimulating the cells with 10 nM CCK.

Despite of the severe fragmentation of the ER in PERK-/- pancreatic acinar cells (Harding et al., 2001), the data showed no significant differences in resting state $[Ca^{2+}]_i$, averaged 77±5 and 69±8 nM in WT and PERK-/- cells; or in peak $[Ca^{2+}]_i$ upon agonist stimulation, which was increased to 515±39 and 509±43 nM in WT and PERK-/- cells, respectively (Fig 5-1A,B). When they were allowed to reload for various lengths of time in the presence of atropine, WT and PERK-/- cells showed no difference in the rate of reloading. Given enough time, both cells were able to fully reload their internal Ca^{2+} stores (Fig 5-1C).

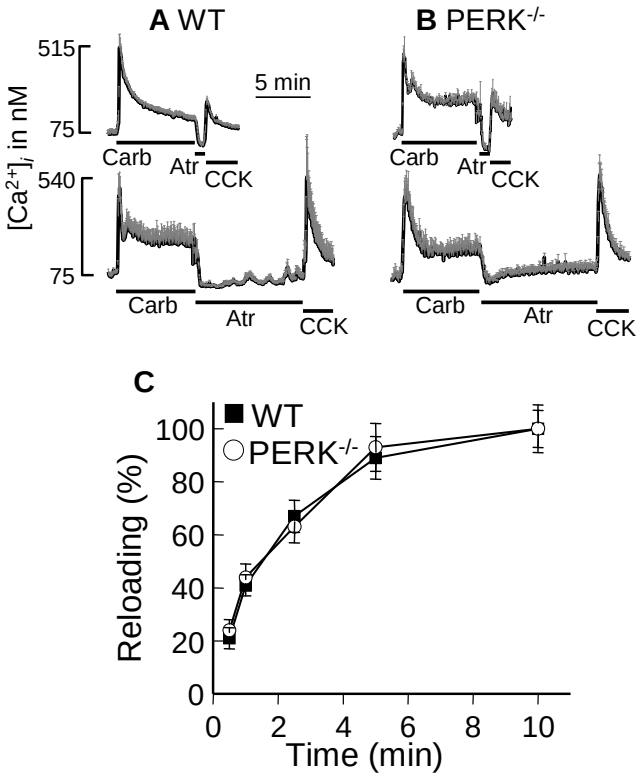

Figure 5-1 ER stress of PERK$^{-/-}$ cells does not affect reloading of the internal Ca^{2+}-stores.
WT (A) and PERK$^{-/-}$ (B) pancreatic acini were stimulated with 1 mM carbachol to discharge the agonist-mobilizable intracellular Ca^{2+} pool. Reloading was initiated by termination of the stimulation with 10 μM atropine. At different times after initiation of reloading, the cells were re-stimulated with 10 nM CCK to estimate the extent of reloading, which was calculated as percentage of the maximal response measured with cells stimulated only with CCK. The upper and lower traces in (A) and (B) show the reloading after 30 sec and 10 min treatment with atropine and the time courses of reloading are plotted in panel (C) for WT (■) and PERK-/- (○) cells. The traces and the summary in (C) is the mean (black trace) ±S.E.M. (gray lines) of at least three experiments.

When pancreatic acinar cells were stimulated with carbachol, the most noticeable difference between WT and PERK-/- cells is the rate of Ca^{2+} release. Cellular $[Ca^{2+}]_i$ elevation in PERK-/- was significantly slower than that in WT when stimulated with 5 and 25 μM carbachol (Fig 5-2A). This difference in Ca^{2+} release rate is reduced with increasing concentration of the agonist until completely disappeared at 1 mM carbachol, as summarized in Fig 5-2B. In contrast, the peak $[Ca^{2+}]_i$ following stimulation is unaltered in PERK-/- cells compared with WT cells within 1 – 1000 μM of carbachol (Fig 5-2C) **.**

When these experiments were repeated in the absence of $[Ca^{2+}]_o$, similar results were observed, suggesting that delayed Ca^{2+} elevation in PERK-/- cells is due to delayed Ca^{2+} release from intracellular stores.

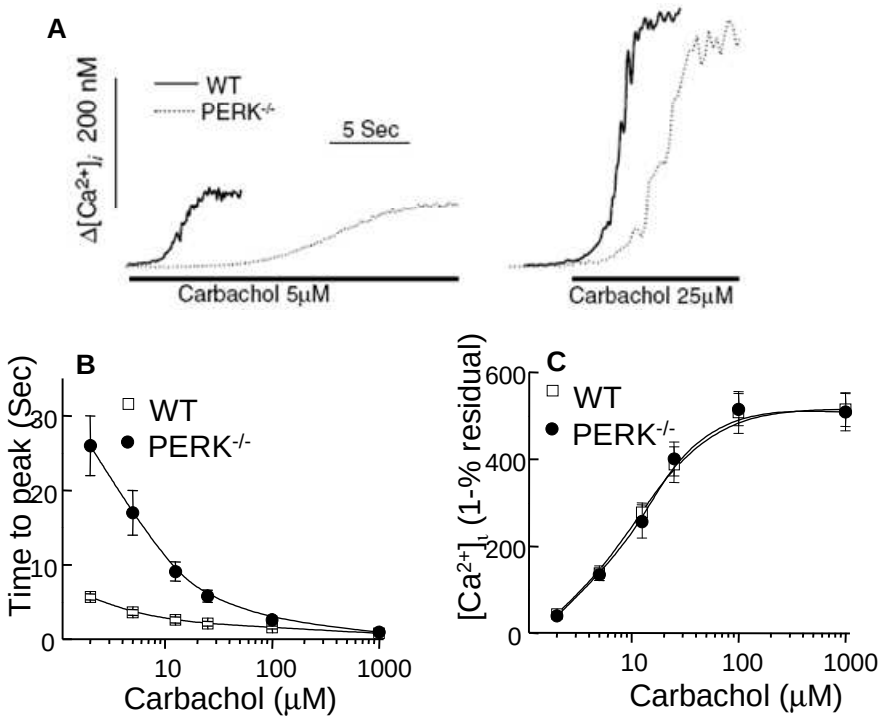

Figure 5-2 Fragmentation of the ER reduces the rate of $[Ca^{2+}]_i$ increase.

(A) Examples of the Ca^{2+} increase in individual pancreatic acini obtained from WT (solid traces) and $PERK^{-/-}$ mice (dashed traces) and stimulated with 5 μM carbachol. WT (■) and $PERK^{-/-}$ (○) pancreatic acinar cells were stimulated with different concentrations of carbachol and the extent (B) and rate (C) of the $[Ca^{2+}]_i$ increase were measured. The results are the mean±S.E.M. of three experiments.

As mentioned in the introduction, apical-to-basal Ca^{2+} wave is a typical Ca^{2+} event in polarized acinar cell. It highly relies on IP_3 to mobilize Ca^{2+} release machinery and Ca^{2+}-induced-Ca^{2+} release mechanism. Presumably, the disrupted ER morphology will cause change in the pattern of Ca^{2+} wave. When treated with 5 μM carbachol, PERK-/- cells lacked an apical-to-basal Ca^{2+} wave. Instead, both the apical and basal regions saw slow $[Ca^{2+}]_i$ increase at about the same rate (Fig 5-3A,C). When the concentration of carbachol was raised to 100 and above, in some PERK-/- cells, an apical-to-basal Ca^{2+} wave was observed (Fig 5-3B,C). Although both in WT and PERK-/- cells, the rate of the propagation of Ca^{2+} wave increased in proportion to the concentration of the agonist, the rate was significantly slower in PERK-/- cells stimulated by 100 μM carbachol. When stimulated with 1 mM carbachol, PERK-/- cells demonstrated Ca^{2+} wave similar to WT cells (Fig 5-3D).

These findings suggest that the integrity of ER does not seem to be critical when concentration of Ca^{2+}-mobilizing agonist is high. However, at lower concentration of agonist, the integrity of ER plays an important role in relaying the Ca^{2+}-releasing signals. The observation of compensation of defective Ca^{2+} release by high concentration of agonist in PERK-/- cells suggests that the defect in Ca^{2+} regulation lies in the efficiency of the transduction of signals.

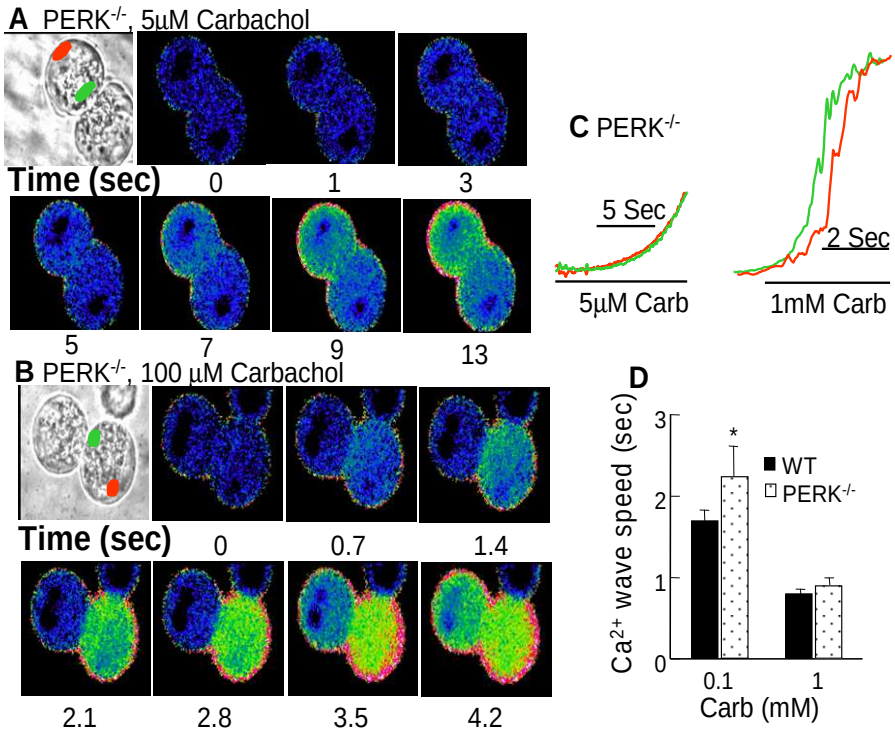

Figure 5-3 Ca^{2+} waves in $PERK^{-/-}$ pancreatic acinar cells.

$PERK^{-/-}$ pancreatic acinar cells were stimulated with the indicated concentrations of carbachol. Selective images of cells stimulated with 5 (A) or 100 μM carbachol (B) and the changes in $[Ca^{2+}]_i$ at the apical (green regions of interest and traces) and basal poles (red regions of interest and traces) are shown in (C). Panel (D) shows the rate of the Ca^{2+} waves recorded in cells stimulated with 0.1 and 1 mM carbachol. The results are the mean ± S.E.M. of 5/11 cells stimulated with 100 μM carbachol that showed a Ca^{2+} wave and of 8/8 cells stimulated with 1 mM carbachol (Carb).

5.3 Expression and responsiveness of the IP_3R pathway is unaltered

Production of IP_3 is the initial step in agonist-evoked Ca^{2+} release in acinar cell. Pancreatic acinar cells were incubated with 2, 20, 50, or 1000 μM of cabarchol respectively. When normalized by cellular protein mass, PERK-/- cell was equally potential as WT in IP_3 production (Fig 5-4A). Surprisingly, the result was not agonist dependent as evident by CCK and BS stimulation (Fig 5-4B). Deletion of PERK showed no effect on IP_3 production by either stimulant.

An important question is whether the slow Ca^{2+} release is caused by altered intracellular distribution or responsiveness of IP_3 receptors. Immunolocalization analysis showed normal distribution of all three subtypes of IP_3Rs in the apical pole in PERK-/- pancreatic cells (Fig 5-4C). To assess IP_3R response directly, pancreatic cells were permeabilize with streptolysine O to allow exogenous IP_3 to access native IP_3Rs. Five successive addition of IP_3 increased the concentration of IP_3 in the incubation by 0.15 μM each time, followed by a final 5 μM increase in IP_3. Surprisingly, there was no difference between the IP_3- mobilized Ca^{2+} stores in the PERK-/- and WT cells in term of the rate of Ca^{2+} release and the magnitude of response (Fig 5-5A, B).

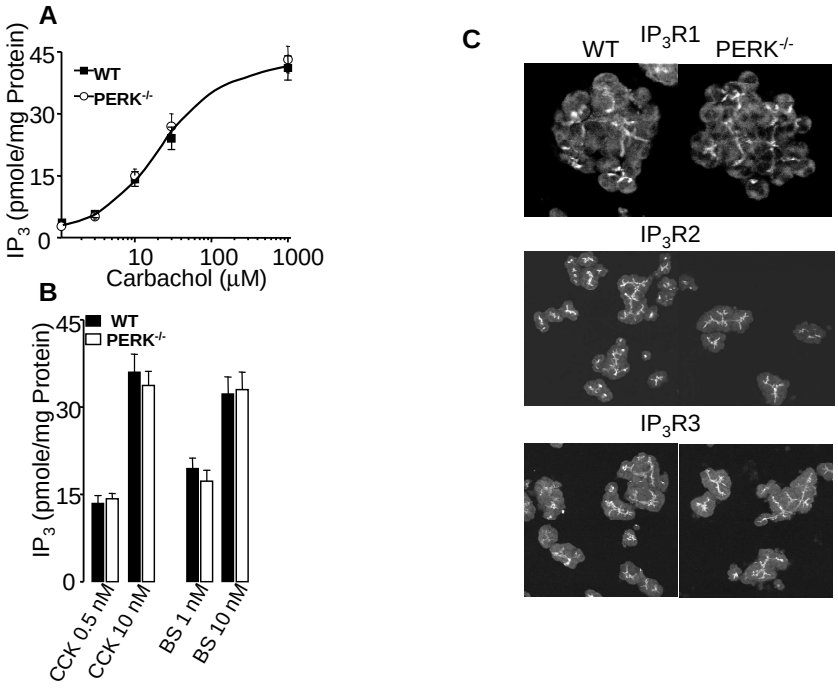

Figure 5-4 Deletion of PERK does not affect IP_3 production, localization of IP_3Rs.
(A, B) WT (filled symbols and columns) and $PERK^{-/-}$ pancreatic acini (open symbols and columns) were stimulated with the indicated concentrations of carbachol (A), CCK or Bombesin (B) for 2-10 sec and the mass of 1, 4, 5 IP_3 was measured. In (C), pancreatic acini were fixed and used for immunolocalization of IP_3R1 (upper images), IP_3R2 (middle images) or IP_3R3 (bottom images) in WT and $PERK^{-/-}$ cells.

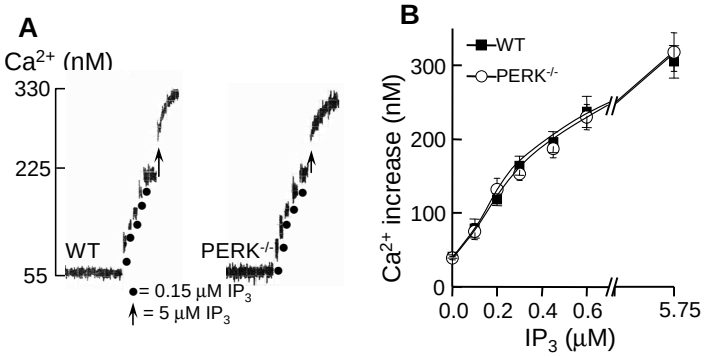

Figure 5-5 Deletion of PERK does not affect IP_3-mediated Ca^{2+} release in pancreatic acinar cells.

(A) pancreatic acini from WT and $PERK^{-/-}$ mice were permeabilized with Streptolysin O and after stabilization of medium Ca^{2+} at about 55 nM increasing concentrations of IP_3 were added to the incubation medium to measure the potency of IP_3 to release Ca^{2+} from the ER (●=addition of 0.15 µM IP_3; ↑=addition of 5 µM IP_3). The results of 3 experiments are summarized in (B) and are given as the mean ± S.E.M. .

5.4 Impaired Ca^{2+}-induced Ca^{2+} release

A rapid propagating Ca^{2+} wave has two components, an initial Ca^{2+} release from IP_3 sensitive stores and a secondary Ca^{2+} release by a mechanism called CICR (Ca^{2+}-induced Ca^{2+} release). CICR in acinar cells is believed to be conducted by ryanodine receptors (RyRs) in a subgroup of Ca^{2+} store, which is functionally distinct from the IP_3 sensitive stores. In general, CICR occurs deeper in the cytosol compared with the apical-localized Ca^{2+} release evoked by IP_3. Since in PERK-/- cells, the signaling that is proximal to IP_3 production seems to be normal, the defect that causes the slow Ca^{2+} release is most likely to lie in the CICR machinery.

Parotid acinar cells were perfused with Solution A containing 0 mM or 7.5 mM Ca^{2+} alternately in the continuous presence of 1 mM carbachol. Alternatively, 10 μM of Ca^{2+} store depleting reagent CPA was used to produce CICR (Fig 5-6 C, D). The most noticeable difference is that the first CICR peak is higher in WT than in PERK-/- cells when treated with carbachol (493±38 and 372±44 nM, n=6) or CPA (403±37 and 312±35 nM, n=5) (Fig 5-6 A-D, E). By contrast, the second CICR peaks, and even the third peaks when treated with CPA, were higher in PERK-/- cells. Ratios between the first and second CICR peaks of the same cell when treated with carbachol or the first and third peaks when treated with CPA were summarized in Fig 5-6F.

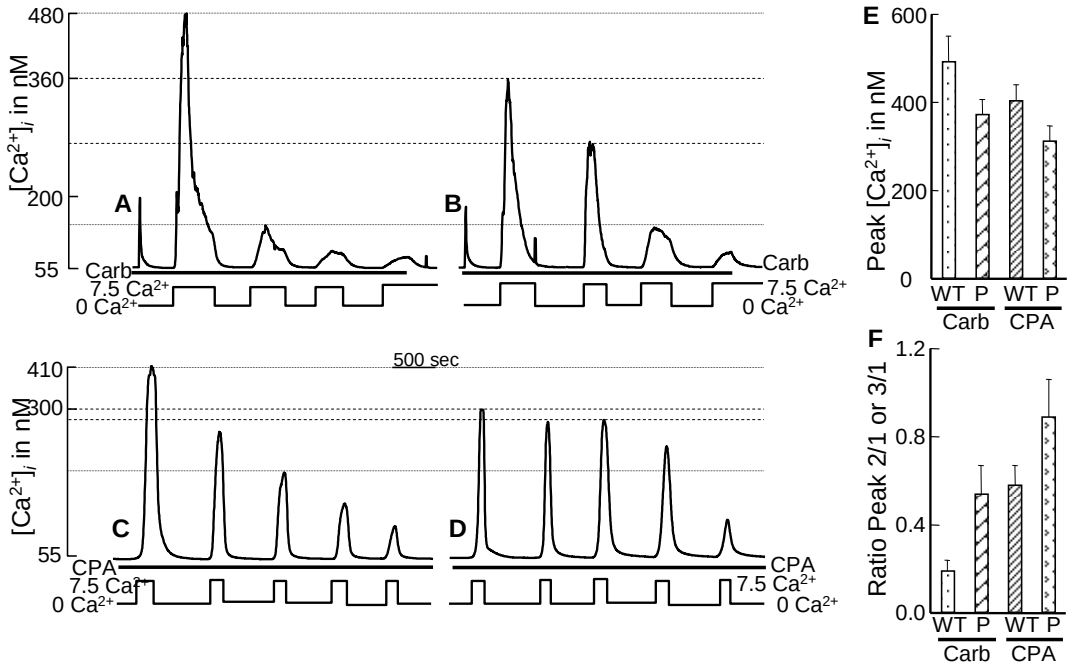

Figure 5-6 Ca^{2+}-induce Ca^{2+} release in WT and $PERK^{-/-}$ parotid acini.

WT (A, C) and $PERK^{-/-}$ parotid acini (B, D) were incubated in Ca^{2+}-free medium and either stimulated with 1 mM carbachol (A, B) or treated with 10 μM CPA for 2 minutes. Then the acini were alternately exposed to medium containing 7.5 or 0 mM Ca^{2+} to induce CICR. The averaged peak increases in $[Ca^{2+}]_i$ are summarized in (E). The ratios between the first and second peaks (carbachol stimulation) and first and third peak (CPA treatment) evoked by addition of 7.5 mM Ca^{2+} to WT (doted lines) and $PERK^{-/-}$ cells (dashed lines) are summarized in (F). Summaries are from at least 4 experiments each and are given as the mean ± S.E.M. .

Both carbachol and CPA cause depletion of intracellular Ca^{2+} stores in the absence of extracellular Ca^{2+} and the Ca^{2+} influx that follows the addition of extracellular Ca^{2+} evokes CICR. The above findings suggest that the first CICR event was weaker in PERK-/- cells and left more Ca^{2+} in the CICR stores. Therefore, a few stronger successive CICR events, compared with the WT counterpart, are needed to completely deplete the stores.

To further assess the defect in CICR, I measured the contraction force of urinary bladder smooth muscle (UBSM). In UBSM, contraction is mediated by a mechanism called excitation-contraction coupling (E-C coupling), which involves $Ca_V1.2$ L-type calcium channel and RyR2 (Morimura et al., 2006; Wegener et al., 2004). Membrane depolarization first activates Ca^{2+} influx through $Ca_v1.2$. Ca^{2+} that enters the cell in this manner induces CICR by RyR2. Therefore, measuring the contraction is a way to assess CICR in UBSM instead of direct Ca^{2+} imaging.

20, 40 or 60 mM K^+ was added to the muscle strips to induce membrane depolarization and contraction. At 20 mM K^+, contraction force was barely detectable in PERK-/- muscle compared with a small yet measurable contraction in WT. At 40 mM K^+, force in PERK-/- UBSM was still significantly weaker than that in WT UBSM. The different in contraction force disappeared when muscle strips were exposed to 80 mM extracellular K^+ (Fig 5-7 A, B).

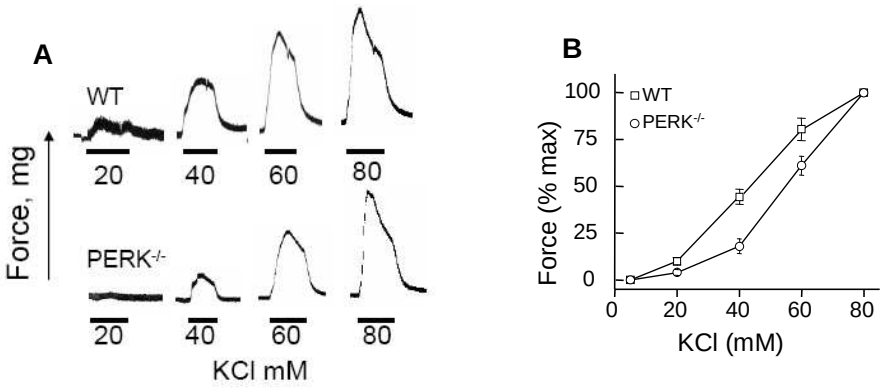

Figure 5-7 Depolarization induced contraction in urinary bladder smooth muscle strips. Panel (A) shows the changes in force in UBSM strips from WT (upper traces) and PERK$^{-/-}$ mice (lower traces) depolarized with 20-80 mM K^+. The average force increases in 3 WT (■) and 3 PERK$^{-/-}$ (○) mice are summarized in (D), and are given as the mean ± S.E.M.. The responses were calculated as percentage of those induced by 80 mM KCl in each strip.

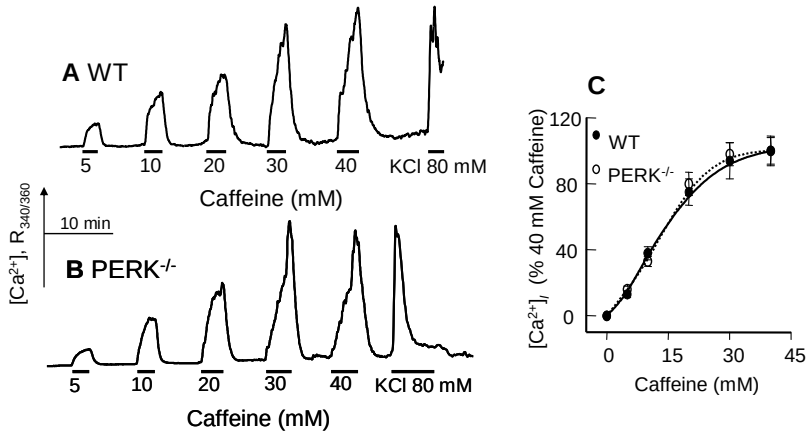

Figure 5-8 Caffeine-induced Ca^{2+} release in WT and $PERK^{-/-}$ urinary bladder smooth muscle cells.

WT (A) and $PERK^{-/-}$ UBSM strips (B) were exposed to caffeine concentrations between 5-40 mM and then depolarized with 80 mM K^+ to measure the activity of the RyRs in the UBSM. The response of 4 strips from 2 WT and 2 $PERK^{-/-}$ mice are averaged in (C) and are given as the mean ± S.E.M.

Reduced contractile response implies impaired CICR in PERK-/- UBSM. Direct imaging of $[Ca^{2+}]_i$ changes in UBSM performed by my colleagues also confirmed my observation. Moreover, electrophysiology data indicated that the function of $Ca_v1.2$ is not significantly affected in PERK-/- cell, including the time course of the $Ca_v1.2$ current and the voltage dependence of activation and current density. Thus it is hypothesized that the conductivity of RyR2 is downregulated by the abnormalities of ER, in which RyRs are residing.

WT and PERK-/- UBSM strips were then treated with increasing concentration of caffeine (5- 40 mM), an activator of RyRs. Data showed that RyRs in PERK-/- UBSM were as responsive as that in WT (Fig 5-8). Since functions of both $Ca_v1.2$ and RyRs are apparently unaltered, the result resembled that of reduced rate of IP_3-mediated Ca^{2+} release. All components are normal yet the output is weaker. The most likely reason is that the disrupted microdomain somehow delays the transduction of signals.

5.5 Disrupted structure of Ca^{2+} microdomains in PERK-/- cells

In signal transduction, soluble ligands often need to travel to its target receptors to relay the signal. For example, during hormone induced Ca^{2+} release from ER, IP_3 diffuses from PM to ER to activate IP_3Rs. In CICR diffusion of calcium ion entering through $Ca_v1.2$ to ER is necessary to activate RyRs. To investigate the extent of microdomain disruption, we designed co-immunoprecipitation experiments to assess the co-expression of IP_3R3, PMCA and SERCA2b in pancreatic acini and that of $Ca_v1.2$ and RyR2 in UBSM. From the results obtained by Guojing Huang in our lab, it is clear that PMCA co-immunoprecipitates with IP_3R3 and SERCA2b in WT acini (Shin et al., 2000). As

demonstrated in Fig 5-9, deletion of PERK did not affect the expression of PMCA and IP_3R3, and slightly reduced expression of SERCA2b. However, the interaction was nearly abolished in PERK-/- cells.

It is evident from previous studies that in UBSM muscles, $Ca_v1.2$ and RyR2 interact through scaffold protein Homer1(Huang et al., 2007). Expression of $Ca_v1.2$ and RyR2 in PERK-/- UBSM was only slightly increased, but the interaction between $Ca_v1.2$ and RyR2 was greatly reduced. Biochemistry data validated the hypothesis that overstressed distended/fragmented ER disrupted the integrity of PM/ER microdomain, resulting in reduced efficiency in transduction of signals and reduced Ca^{2+} release. This also explained the observation that at higher concentration of stimuli, the reduced signal transduction is alleviated. The higher initial concentration of second messengers compensated for the larger distance they need to diffuse across.

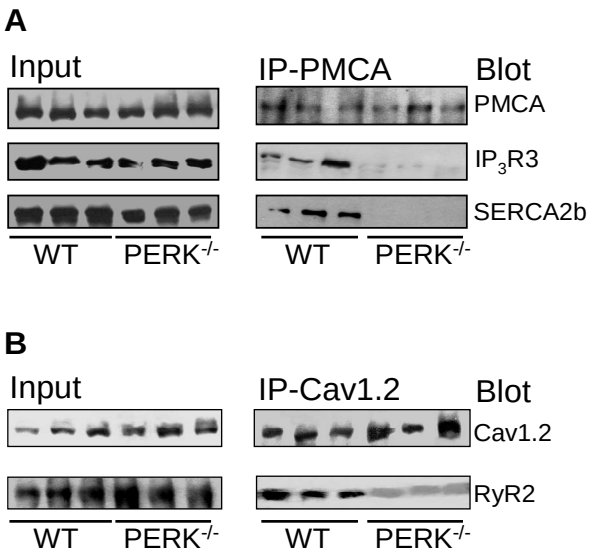

Figure 5-9 co-IP of plasma membrane and ER residing proteins in WT and PERK$^{-/-}$ cells.
In (A) extracts from pancreatic acini of 3 WT and 3 PERK$^{-/-}$ mice were used to measure expression (input) of the indicated proteins and for immunoprecipitation of PMCA. The immunoprecipitates were analyzed for co-IP of PMCA, IP_3R3 and SERCA2b. In (B) extracts from UBSM of 3 WT and 3 PERK$^{-/-}$ mice were used to measure expression of the indicated proteins and for immunoprecipitation of $Ca_v1.2$. The immunoprecipitates were analyzed for co-IP of $Ca_v1.2$ and RyR2.

ER is not only the site of protein synthesis and post translational processing, but also a major regulator that orchestrate Ca^{2+} signaling. Abnormal Ca^{2+} load in ER affect processing of proteins. On the other hand, ER stress posed by protein overload affects the regulatory functions of ER in $Ca2^{+}$ signaling. In this study I have identified an intriguing defect in Ca^{2+} signaling in $PERK^{-/-}$ knockout cells: chronic ER stress reduces the rate and efficiency of Ca^{2+} release from the IP_3 and CICR responsive store. This defect explains the decline in secretory cell functions. These findings establish a relationship between the unfolded protein response, ER stress and Ca^{2+} signaling and highlight the importance of communication within the PM-ER microdomain for propagation of the Ca^{2+} signal from the plasma membrane into the cell.

Chapter 6 Summary and Future Directions

Near plasma membrane Ca^{2+} microdomain has been shown to exist in excitable cells like neuron and muscle cells. Studies of Ca^{2+} microdomain in such cells have greatly advanced our understanding of the regulation mechanism and physiological implication of Ca^{2+} dynamics. However, in non-excitable cells such as exocrine acinar cells, direct evidence of such microdomain is absent. The goal of my study is to characterize the properties of such microdomain and explore its physiological relevance in the context of the secretory functions of exocrine acinar cells.

An array of biophysical approaches including fluorescent imaging and patch clamping has been widely used to record Ca^{2+} dynamics. A relatively newly developed technique is the Total Internal Reflection Fluorescence Microscopy (TIRFM). The strength of TIRFM is its superior focus on a narrow strip of space right under cell membrane. This small slice of cytoplasm is also where the near plasma membrane microdomains locate. By combining this technique with whole-field fluorescence imaging, I was able to examine and quantify the change of the concentration of free Ca^{2+} ion in the bulk cytosol ($\Delta[Ca^{2+}]_{Cyto}$) and in the near membrane microdomains ($\Delta[Ca^{2+}]_{PM}$) in acinar cells. My experiments revealed that $\Delta[Ca^{2+}]_{PM}$ is about 3-fold larger than $\Delta[Ca^{2+}]_{Cyto}$ under supramaximal agonist stimulation, this difference is alleviated by removal of external Ca^{2+}, while resting $[Ca^{2+}]_{PM}$ and $[Ca^{2+}]_{Cyto}$ show no difference. Near membrane microdomains also show greater Ca^{2+} influx regardless the store depletion is induced by activating receptor or by inhibiting SERCA pump.

In response to physiological strength of stimulation, Ca^{2+} oscillation in acinar cells showed dramatically different dynamics between the two compartments. Compared with $[Ca^{2+}]_{PM}$, $[Ca^{2+}]_{Cyto}$ oscillations last longer in Ca^{2+} free media but recovered more slowly after re-addition of external Ca^{2+}. My data also revealed that ionomycin, a potent ionophore, evoked less robust and shorter lasting elevation of $[Ca^{2+}]_{PM}$ compared with $[Ca^{2+}]_{Cyto}$.

These data validate the existence of near plasma membrane microdomains in non-excitable exocrine acinar cell. The fact that $[Ca^{2+}]_{PM}$ and $[Ca^{2+}]_{Cyto}$ differ in many ways under stimulation suggests that the microdomain is the signaling platform and the "hot spot" of Ca^{2+} entering the cytosol. Recently, great stride has been made in identifying molecular entities of long time evasive components in store-operated Ca^{2+} influx pathway. These include Orai1 that was found to be the pore forming unit of I_{CRAC} and STIM1 that was revealed to be the critical molecule that senses the depletion of Ca^{2+} in ER stores and transmits the signal to channels in the plasma membrane.

To extend the current studies on the Ca^{2+} dynamics near plasma membrane microdomain, the role played by each of these essential molecules, including Orai1, STIM1 and TRPC channels, can be further analyzed. The ideal model system is exocrine acinar cells from viable mice that carry knock-out or mutations of the genes of interest, since culturing of functional primary acinar cells is not available at present. It is also interesting to study the near plasma membrane microdomain in cultured cell lines, such as Hela and 293T cells. The cultured cells would enable us to use either overexpression or gene-knock out by siRNA to study the interaction and functions of individual

components. For all these systems, TIRFM could be easily applied to record the rapid Ca^{2+} signals in the near plasma membrane.

Microdomain is a transient signaling complex that renders high local [Ca^{2+}] affecting only neighboring effectors, a feature desired by many cellular processes; one of such is Ca^{2+}-induced Ca^{2+} release (CICR). RyRs mediating CICR is already well established in cardiac and skeletal muscles. By contrast, the activation mechanism of CICR in non-muscle cells remains unclear.

My study was the first to demonstrate CICR in parotid acinar cell. Stimulating cell in Ca^{2+} free media showed that 0.5 μM carbachol releases ~5% of the Ca^{2+} mobilizable by 1mM carbachol. Addition of external Ca^{2+} induces the same explosive and robust Ca^{2+} release in both cases. Similar results were observed by treating the cell with CPA, a SERCA inhibitor, for short periods of time to passively deplete the stores. The measurement of Mn^{2+} influx demonstrated that the magnitude of Ca^{2+} influx is proportional to the extent of receptor activation / store depletion. Collectively, minimal activation of Ca^{2+} influx by partial store depletion results in an explosive mobilization of Ca^{2+} from the majority of the stores by CICR.

The Ca^{2+} influx in parotid acinar cell is likely to be conducted by cell surface SOC channels and explosive Ca^{2+} release from stores is largely independent of IP3Rs as revealed by pharmacological experiments. These findings demonstrate a previously unrecognized role for Ca^{2+} influx in non-excitable cells and suggest that CICR in parotid acinar cells resembles CICR in cardiac muscle with the exception that in cardiac myocytes Ca^{2+} influx is mediated by voltage-operated Ca^{2+} channels whereas in non-excitable cells Ca^{2+} influx is mediated by store-operated channels.

The evidence in this study supporting RyRs as the mediator of the secondary Ca^{2+} release is indirect. I have used caffeine, a potent RyR activator in muscle cells, on the acinar cells and observed no significant effects. Alternatively, I may use ruthenium red as a blocker to the RyRs to inhibit secondary Ca^{2+} release. If Ca^{2+} release is truly carried out through RyRs, then ruthenium red at nanomolar concentrations will be able to block CICR following the store depletion.

In muscles, the essential role of CICR in excitation-contraction coupling is well established. It is evident that CICR by activation of RyRs is essential to receptor-evoked Ca^{2+} signaling, but consensus is lacking on the physiological relevance of CICR in non-excitable cells as well as which isoform(s) of RyR is responsible for the Ca^{2+} release from Ca^{2+} stores. My hypothesis is that CICR may be essential in generating receptor-specific Ca^{2+} signals. Measurement of the response to several concentration of CPA revealed that the total content of Ca^{2+} stores is unchanged regardless the degree of activation of Ca^{2+} influx. This result indicates that only a small and selective portion of internal stores has the potential to activate Ca^{2+} influx hence to trigger CICR. The small portion of store may participate in the near plasma membrane microdomain that is organized around each individual or group of GPCR. Thus, the activation of receptor results in activation of its associated internal stores, influx channel and RyR. To further understand the regulation of CICR in acinar cell, identification of the SOCs and RyR isoforms that are involved is critical.

Experiment results also revealed that most CICR triggered by Ca^{2+} influx occurred away from the plasma membrane. It is not clear what role the Ca^{2+} released in this manner plays. I proposed a working model that describes the CICR propagates

inward as a cascade of Ca^{2+} release until the signal reaches its target of regulation, possibly expression of genes or modification of secretory pathway. It is equally unclear whether the propagation of CICR is receptor specific. These aspects are worth investigating in the future.

The third part of my study is on the effects of chronic ER stress on Ca^{2+} signaling. The most intriguing discovery was that ER stress induced by PERK mutation impeded both the efficiency and fidelity of Ca^{2+} signaling. In PERK-/- pancreatic acinar cell, both IP3 production evoked by activation of GPCR and the responsiveness of IP3 sensitive Ca^{2+} stores were unaltered; yet Ca^{2+} was released at a reduced rate following stimulation of the cell. It appeared that the defect lies in the steps between IP3 production and IP3-mediated Ca^{2+} release. Similarly, in PERK-/- urinary bladder smooth muscle, the responsiveness of CICR was weakened while the activity of upstream $Ca_v1.2$ and downstream RyRs was unchanged.

It is fair to postulate that chronic ER stress-induced fragmentation and distension of ER delays the transduction of signals from cell membrane microdomain to ER microdomain. In another word, it could be the impaired communication in the near plasma membrane microdomain that causes defects in the Ca^{2+} signaling. Indeed, the biochemistry data supported such hypothesis. Co-immunoprecipitation experiments showed reduced interaction between plasma membrane residing protein and ER residing proteins in both acinar cell and in UBSM. If this is the mechanism underlying the defective Ca^{2+} signaling in PERK-/-, the existence and functional significance of the near plasma membrane microdomain is confirmed.

The other possibility is that PERK mutation affects expression of genes required for Ca^{2+} signaling, since PERK is involved in the regulation of expression of genes that regulate many cellular processes. In this case, a genome wide screen using gene chips can provide data to help distinguish these two possibilities. In both scenarios, the molecular basis of defect in Ca^{2+} signaling in PERK-/- cells remains to be explored.

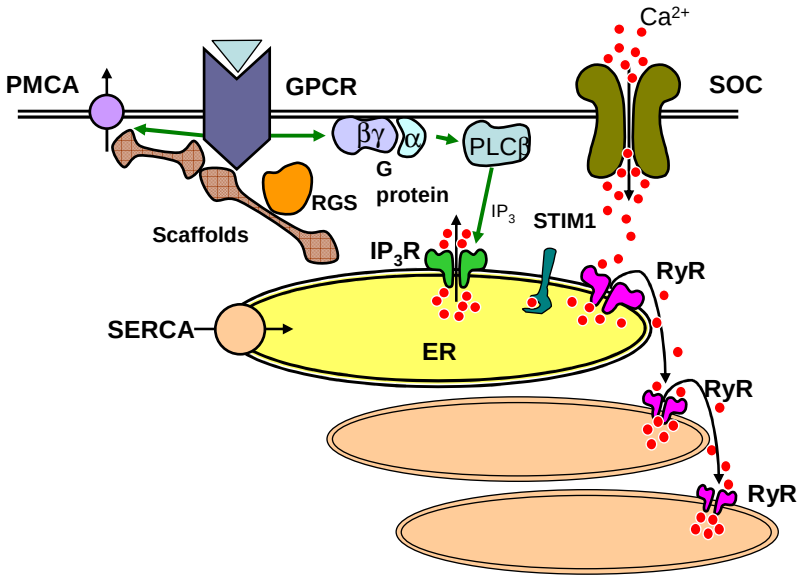

Figure 6-1 Working model of Ca^{2+} signaling transduction in the PM-ER microdomain of acinar cells.

Red dots represent free Ca^{2+} ions. Green arrows indicate activation; black arrows indicate direction of Ca^{2+} movement. PM-ER microdomain is assembled and activated upon agonist binding, affecters and effecters interact directly or indirectly through the assistant of scaffolding proteins. Proper positioning of the components is vital for the functions of microdomain. Ca^{2+} influx through the SOC channel induces a cascade of Ca^{2+} discharges by the CICR mechanism, resulting in effective transmission of signals deep into the cytoplasm.

Part of my result is summarized in the working model as illustrated in Figure 6-1. Calcium signaling is regulated precisely in both spatial and temporal dimension. How to capture [Ca^{2+}] change faithfully over different period of time and into different depth of cell is essential in the study of Ca^{2+} signaling. This poses a great challenge for investigation and calls a combination of new advance techniques. In the current study, I used both TIRFM and wide-field fluorescent imaging to understand the regulation of Ca^{2+} microdomain in live acinar cells. In the future, novel fusion protein that could be targeted to specific cellular location can be used to assess the transient interaction between different components in the microdomain. Novel probes suitable for measuring high [Ca^{2+}] with better dynamic characteristics are useful in measuring localized [Ca^{2+}] transients (Giacomello et al., 2010; Pham and Truong, 2010). Moreover, recent progress in super-resolution fluorescence microscopy techniques, which resolve beyond 200nm, brings about the hope that more details of complex subcellular structures can be acquired and analyzed (Betzig et al., 2006; Klar et al., 2000; Rust et al., 2006; Schuldt, 2010) .

Study of Ca^{2+} signaling is a fast-evolving field; new knowledge is added every day on how Ca^{2+} functions in cell. My dissertation study only touched a very specific topic:

microdomain in non-excitable acinar cell. I believe my findings add insights into our understanding of the regulation of Ca^{2+} signaling. The discovery made in acinar cell may be universal in non-excitable cells. More importantly, knowing the components in microdomain functioning in a transient manner expands the scope of future investigations. Molecular mechanisms of assemble and dissemble of the microdomains shall be of interest. Accumulating knowledge of domains that mediate activation, inactivation, translocation, interaction and recycling of individual molecular components will bring new insights into how the signaling complex is orchestrated. Structural information of STIM1, Orai1 and TRP channels will also shed new light on the regulatory mechanisms.

Bibliography

Ahn, W., Lee, M. G., Kim, K. H., and Muallem, S. (2003). Multiple effects of SERCA2b mutations associated with Darier's disease. J Biol Chem *278*, 20795-20801.

Arai, M., Alpert, N. R., MacLennan, D. H., Barton, P., and Periasamy, M. (1993). Alterations in sarcoplasmic reticulum gene expression in human heart failure. A possible mechanism for alterations in systolic and diastolic properties of the failing myocardium. Circ Res *72*, 463-469.

Aridor, M., and Balch, W. E. (1999). Integration of endoplasmic reticulum signaling in health and disease. Nat Med *5*, 745-751.

Baba, Y., Hayashi, K., Fujii, Y., Mizushima, A., Watarai, H., Wakamori, M., Numaga, T., Mori, Y., Iino, M., Hikida, M., and Kurosaki, T. (2006). Coupling of STIM1 to store-operated Ca2+ entry through its constitutive and inducible movement in the endoplasmic reticulum. Proc Natl Acad Sci U S A *103*, 16704-16709.

Berridge, M. J. (1993). Inositol trisphosphate and calcium signalling. Nature *361*, 315-325.

Berridge, M. J., Bootman, M. D., and Roderick, H. L. (2003). Calcium signalling: dynamics, homeostasis and remodelling. Nat Rev Mol Cell Biol *4*, 517-529.

Berridge, M. J., Heslop, J. P., Irvine, R. F., and Brown, K. D. (1984). Inositol trisphosphate formation and calcium mobilization in Swiss 3T3 cells in response to platelet-derived growth factor. Biochem J *222*, 195-201.

Berridge, M. J., Lipp, P., and Bootman, M. D. (2000). The versatility and universality of calcium signalling. Nat Rev Mol Cell Biol *1*, 11-21.

Bers, D. M. (2002). Cardiac excitation-contraction coupling. Nature *415*, 198-205.

Betzig, E., Patterson, G. H., Sougrat, R., Lindwasser, O. W., Olenych, S., Bonifacino, J. S., Davidson, M. W., Lippincott-Schwartz, J., and Hess, H. F. (2006). Imaging intracellular fluorescent proteins at nanometer resolution. Science *313*, 1642-1645.

Bezprozvanny, I., and Ehrlich, B. E. (1994). Inositol (1,4,5)-trisphosphate (InsP3)-gated Ca channels from cerebellum: conduction properties for divalent cations and regulation by intraluminal calcium. J Gen Physiol *104*, 821-856.

Bezprozvanny, I., Watras, J., and Ehrlich, B. E. (1991). Bell-shaped calcium-response curves of Ins(1,4,5)P3- and calcium-gated channels from endoplasmic reticulum of cerebellum. Nature *351*, 751-754.

Brini, M., and Carafoli, E. (2009). Calcium pumps in health and disease. Physiol Rev *89*, 1341-1378.

Cahalan, M. D. (2009). STIMulating store-operated Ca(2+) entry. Nat Cell Biol *11*, 669-677.

Dziadek, M. A., and Johnstone, L. S. (2007). Biochemical properties and cellular localisation of STIM proteins. Cell Calcium *42*, 123-132.

Fill, M., and Copello, J. A. (2002). Ryanodine receptor calcium release channels. Physiol Rev *82*, 893-922.

Fitzsimmons, T. J., Gukovsky, I., McRoberts, J. A., Rodriguez, E., Lai, F. A., and Pandol, S. J. (2000). Multiple isoforms of the ryanodine receptor are expressed in rat pancreatic acinar cells. Biochem J *351*, 265-271.

Franzini-Armstrong, C., and Protasi, F. (1997). Ryanodine receptors of striated muscles: a complex channel capable of multiple interactions. Physiol Rev *77*, 699-729.

Frieden, M., Arnaudeau, S., Castelbou, C., and Demaurex, N. (2005). Subplasmalemmal mitochondria modulate the activity of plasma membrane Ca2+-ATPases. J Biol Chem *280*, 43198-43208.

Giacomello, M., Drago, I., Bortolozzi, M., Scorzeto, M., Gianelle, A., Pizzo, P., and Pozzan, T. (2010). Ca2+ hot spots on the mitochondrial surface are generated by Ca2+ mobilization from stores, but not by activation of store-operated Ca2+ channels. Mol Cell *38*, 280-290.

Harding, H. P., Zeng, H., Zhang, Y., Jungries, R., Chung, P., Plesken, H., Sabatini, D. D., and Ron, D. (2001). Diabetes mellitus and exocrine pancreatic dysfunction in perk-/- mice reveals a role for translational control in secretory cell survival. Mol Cell *7*, 1153-1163.

Harding, H. P., Zhang, Y., Bertolotti, A., Zeng, H., and Ron, D. (2000). Perk is essential for translational regulation and cell survival during the unfolded protein response. Mol Cell *5*, 897-904.

Harding, H. P., Zhang, Y., and Ron, D. (1999). Protein translation and folding are coupled by an endoplasmic-reticulum-resident kinase. Nature *397*, 271-274.

Hoth, M., and Penner, R. (1992). Depletion of intracellular calcium stores activates a calcium current in mast cells. Nature *355*, 353-356.

Huang, G., Kim, J. Y., Dehoff, M., Mizuno, Y., Kamm, K. E., Worley, P. F., Muallem, S., and Zeng, W. (2007). Ca2+ signaling in microdomains: Homer1 mediates the interaction between RyR2 and Cav1.2 to regulate excitation-contraction coupling. J Biol Chem *282*, 14283-14290.

Ji, W., Xu, P., Li, Z., Lu, J., Liu, L., Zhan, Y., Chen, Y., Hille, B., Xu, T., and Chen, L. (2008). Functional stoichiometry of the unitary calcium-release-activated calcium channel. Proc Natl Acad Sci U S A *105*, 13668-13673.

Kiselyov, K., Mignery, G. A., Zhu, M. X., and Muallem, S. (1999). The N-terminal domain of the IP3 receptor gates store-operated hTrp3 channels. Mol Cell *4*, 423-429.

Kiselyov, K., Shin, D. M., Luo, X., Ko, S. B., and Muallem, S. (2002). Ca2+ signaling in polarized exocrine cells. Adv Exp Med Biol *506*, 175-183.

Kiselyov, K., Shin, D. M., and Muallem, S. (2003). Signalling specificity in GPCR-dependent Ca2+ signalling. Cell Signal *15*, 243-253.

Kiselyov, K., Wang, X., Shin, D. M., Zang, W., and Muallem, S. (2006). Calcium signaling complexes in microdomains of polarized secretory cells. Cell Calcium *40*, 451-459.

Klar, T. A., Jakobs, S., Dyba, M., Egner, A., and Hell, S. W. (2000). Fluorescence microscopy with diffraction resolution barrier broken by stimulated emission. Proc Natl Acad Sci U S A *97*, 8206-8210.

Kleizen, B., and Braakman, I. (2004). Protein folding and quality control in the endoplasmic reticulum. Curr Opin Cell Biol *16*, 343-349.

Kostova, Z., and Wolf, D. H. (2003). For whom the bell tolls: protein quality control of the endoplasmic reticulum and the ubiquitin-proteasome connection. EMBO J *22*, 2309-2317.

Lee, B. S., Sessanna, S., Laychock, S. G., and Rubin, R. P. (2002). Expression and cellular localization of a modified type 1 ryanodine receptor and L-type channel proteins in non-muscle cells. J Membr Biol *189*, 181-190.

Lee, H. C. (2000). Multiple calcium stores: separate but interacting. Sci STKE *2000*, pe1.

Lee, H. C. (2004). Multiplicity of Ca2+ messengers and Ca2+ stores: a perspective from cyclic ADP-ribose and NAADP. Curr Mol Med *4*, 227-237.

Lee, M. G., Xu, X., Zeng, W., Diaz, J., Wojcikiewicz, R. J., Kuo, T. H., Wuytack, F., Racymaekers, L., and Muallem, S. (1997). Polarized expression of Ca2+ channels in pancreatic and salivary gland cells. Correlation with initiation and propagation of [Ca2+]i waves. J Biol Chem *272*, 15765-15770.

Leite, M. F., Burgstahler, A. D., and Nathanson, M. H. (2002). Ca2+ waves require sequential activation of inositol trisphosphate receptors and ryanodine receptors in pancreatic acini. Gastroenterology *122*, 415-427.

Liou, J., Fivaz, M., Inoue, T., and Meyer, T. (2007). Live-cell imaging reveals sequential oligomerization and local plasma membrane targeting of stromal interaction molecule 1 after Ca2+ store depletion. Proc Natl Acad Sci U S A *104*, 9301-9306.

Llinas, R., Sugimori, M., and Silver, R. B. (1992). Microdomains of high calcium concentration in a presynaptic terminal. Science *256*, 677-679.

Lodish, H. F. (1999). Molecular Cell Biology (New York Scientific American Books).

Lur, G., Haynes, L. P., Prior, I. A., Gerasimenko, O. V., Feske, S., Petersen, O. H., Burgoyne, R. D., and Tepikin, A. V. (2009). Ribosome-free terminals of rough ER allow formation of STIM1 puncta and segregation of STIM1 from IP(3) receptors. Curr Biol *19*, 1648-1653.

Marsault, R., Murgia, M., Pozzan, T., and Rizzuto, R. (1997). Domains of high Ca2+ beneath the plasma membrane of living A7r5 cells. Embo J *16*, 1575-1581.

Mattson, M. P. (2010). ER calcium and Alzheimer's disease: in a state of flux. Sci Signal *3*, pe10.

Matute, C. Calcium dyshomeostasis in white matter pathology. Cell Calcium *47*, 150-157.

Morimura, K., Ohi, Y., Yamamura, H., Ohya, S., Muraki, K., and Imaizumi, Y. (2006). Two-step Ca2+ intracellular release underlies excitation-contraction coupling in mouse urinary bladder myocytes. Am J Physiol Cell Physiol *290*, C388-403.

Muik, M., Frischauf, I., Derler, I., Fahrner, M., Bergsmann, J., Eder, P., Schindl, R., Hesch, C., Polzinger, B., Fritsch, R., *et al.* (2008). Dynamic coupling of the putative coiled-coil domain of ORAI1 with STIM1 mediates ORAI1 channel activation. J Biol Chem *283*, 8014-8022.

Muller, E. J., Caldelari, R., Kolly, C., Williamson, L., Baumann, D., Richard, G., Jensen, P., Girling, P., Delprincipe, F., Wyder, M., *et al.* (2006). Consequences of depleted SERCA2-gated calcium stores in the skin. J Invest Dermatol *126*, 721-731.

Navedo, M. F., Amberg, G. C., Votaw, V. S., and Santana, L. F. (2005). Constitutively active L-type Ca2+ channels. Proc Natl Acad Sci U S A *102*, 11112-11117.

Neher, E. (1998). Vesicle pools and Ca2+ microdomains: new tools for understanding their roles in neurotransmitter release. Neuron *20*, 389-399.

Park, M. K., Ashby, M. C., Erdemli, G., Petersen, O. H., and Tepikin, A. V. (2001). Perinuclear, perigranular and sub-plasmalemmal mitochondria have distinct functions in the regulation of cellular calcium transport. Embo J *20*, 1863-1874.

Penna, A., Demuro, A., Yeromin, A. V., Zhang, S. L., Safrina, O., Parker, I., and Cahalan, M. D. (2008). The CRAC channel consists of a tetramer formed by Stim-induced dimerization of Orai dimers. Nature *456*, 116-120.

Periasamy, M., and Huke, S. (2001). SERCA pump level is a critical determinant of Ca(2+)homeostasis and cardiac contractility. J Mol Cell Cardiol *33*, 1053-1063.

Pham, E., and Truong, K. (2010). Design of fluorescent fusion protein probes. Methods Mol Biol *591*, 69-91.

Prakriya, M., Feske, S., Gwack, Y., Srikanth, S., Rao, A., and Hogan, P. G. (2006). Orai1 is an essential pore subunit of the CRAC channel. Nature *443*, 230-233.

Rizzuto, R., Duchen, M. R., and Pozzan, T. (2004). Flirting in little space: the ER/mitochondria Ca2+ liaison. Sci STKE *2004*, re1.

Rizzuto, R., Pinton, P., Carrington, W., Fay, F. S., Fogarty, K. E., Lifshitz, L. M., Tuft, R. A., and Pozzan, T. (1998). Close contacts with the endoplasmic reticulum as determinants of mitochondrial Ca2+ responses. Science *280*, 1763-1766.

Rizzuto, R., and Pozzan, T. (2006). Microdomains of intracellular Ca2+: molecular determinants and functional consequences. Physiol Rev *86*, 369-408.

Rust, M. J., Bates, M., and Zhuang, X. (2006). Sub-diffraction-limit imaging by stochastic optical reconstruction microscopy (STORM). Nat Methods *3*, 793-795.

Rutter, G. A., Fasolato, C., and Rizzuto, R. (1998). Calcium and organelles: a two-sided story. Biochem Biophys Res Commun *253*, 549-557.

Schneggenburger, R., and Neher, E. (2000). Intracellular calcium dependence of transmitter release rates at a fast central synapse. Nature *406*, 889-893.

Schuldt, A. (2010). The limits of light. Nat Rev Mol Cell Biol *11*, 678.

Shin, D. M., Dehoff, M., Luo, X., Kang, S. H., Tu, J., Nayak, S. K., Ross, E. M., Worley, P. F., and Muallem, S. (2003). Homer 2 tunes G protein-coupled receptors stimulus intensity by regulating RGS proteins and PLCbeta GAP activities. J Cell Biol *162*, 293-303.

Shin, D. M., Luo, X., Wilkie, T. M., Miller, L. J., Peck, A. B., Humphreys-Beher, M. G., and Muallem, S. (2001). Polarized expression of G protein-coupled receptors and an all-

or-none discharge of Ca2+ pools at initiation sites of $[Ca^{2+}]_i$ waves in polarized exocrine cells. J Biol Chem *276*, 44146-44156.
Shin, D. M., Zhao, X. S., Zeng, W., Mozhayeva, M., and Muallem, S. (2000). The mammalian Sec6/8 complex interacts with Ca(2+) signaling complexes and regulates their activity. J Cell Biol *150*, 1101-1112.

Smyth, J. T., Dehaven, W. I., Jones, B. F., Mercer, J. C., Trebak, M., Vazquez, G., and Putney, J. W., Jr. (2006). Emerging perspectives in store-operated Ca2+ entry: roles of Orai, Stim and TRP. Biochim Biophys Acta *1763*, 1147-1160.

Sneyd, J., Tsaneva-Atanasova, K., Bruce, J. I., Straub, S. V., Giovannucci, D. R., and Yule, D. I. (2003). A model of calcium waves in pancreatic and parotid acinar cells. Biophys J *85*, 1392-1405.

Straub, S. V., Giovannucci, D. R., and Yule, D. I. (2000). Calcium wave propagation in pancreatic acinar cells: functional interaction of inositol 1,4,5-trisphosphate receptors, ryanodine receptors, and mitochondria. J Gen Physiol *116*, 547-560.

Streb, H., Heslop, J. P., Irvine, R. F., Schulz, I., and Berridge, M. J. (1985). Relationship between secretagogue-induced Ca2+ release and inositol polyphosphate production in permeabilized pancreatic acinar cells. J Biol Chem *260*, 7309-7315.

Streb, H., Irvine, R. F., Berridge, M. J., and Schulz, I. (1983). Release of Ca2+ from a nonmitochondrial intracellular store in pancreatic acinar cells by inositol-1,4,5-trisphosphate. Nature *306*, 67-69.

Thorn, P. (1993). Spatial aspects of Ca2+ signalling in pancreatic acinar cells. J Exp Biol *184*, 129-144.

Thorn, P., Gerasimenko, O., and Petersen, O. H. (1994). Cyclic ADP-ribose regulation of ryanodine receptors involved in agonist evoked cytosolic Ca2+ oscillations in pancreatic acinar cells. EMBO J *13*, 2038-2043.

Verkhratsky, A., and Fernyhough, P. (2008). Mitochondrial malfunction and Ca2+ dyshomeostasis drive neuronal pathology in diabetes. Cell Calcium *44*, 112-122.

Wang, X., Zeng, W., Soyombo, A. A., Tang, W., Ross, E. M., Barnes, A. P., Milgram, S. L., Penninger, J. M., Allen, P. B., Greengard, P., and Muallem, S. (2005). Spinophilin regulates Ca2+ signalling by binding the N-terminal domain of RGS2 and the third intracellular loop of G-protein-coupled receptors. Nat Cell Biol *7*, 405-411.

Wegener, J. W., Schulla, V., Lee, T. S., Koller, A., Feil, S., Feil, R., Kleppisch, T., Klugbauer, N., Moosmang, S., Welling, A., and Hofmann, F. (2004). An essential role of Cav1.2 L-type calcium channel for urinary bladder function. FASEB J *18*, 1159-1161.

Worley, P. F., Zeng, W., Huang, G. N., Yuan, J. P., Kim, J. Y., Lee, M. G., and Muallem, S. (2007). TRPC channels as STIM1-regulated store-operated channels. Cell Calcium *42*, 205-211.

Wu, M. M., Buchanan, J., Luik, R. M., and Lewis, R. S. (2006). Ca2+ store depletion causes STIM1 to accumulate in ER regions closely associated with the plasma membrane. J Cell Biol *174*, 803-813.

Wu, S., Hu, Y., Wang, J. L., Chatterjee, M., Shi, Y., and Kaufman, R. J. (2002). Ultraviolet light inhibits translation through activation of the unfolded protein response kinase PERK in the lumen of the endoplasmic reticulum. J Biol Chem *277*, 18077-18083.

Wu, X., Chang, B., Blair, N. S., Sargent, M., York, A. J., Robbins, J., Shull, G. E., and Molkentin, J. D. (2009). Plasma membrane Ca2+-ATPase isoform 4 antagonizes cardiac hypertrophy in association with calcineurin inhibition in rodents. J Clin Invest *119*, 976-985.

Yeromin, A. V., Zhang, S. L., Jiang, W., Yu, Y., Safrina, O., and Cahalan, M. D. (2006). Molecular identification of the CRAC channel by altered ion selectivity in a mutant of Orai. Nature *443*, 226-229.

Young, R. C., and Zhang, P. (2004). Functional separation of deep cytoplasmic calcium from subplasmalemmal space calcium in cultured human uterine smooth muscle cells. Cell Calcium *36*, 11-17.

Yuan, J. P., Zeng, W., Huang, G. N., Worley, P. F., and Muallem, S. (2007). STIM1 heteromultimerizes TRPC channels to determine their function as store-operated channels. Nat Cell Biol *9*, 636-645.

Zenisek, D., Steyer, J. A., and Almers, W. (2000). Transport, capture and exocytosis of single synaptic vesicles at active zones. Nature *406*, 849-854.

Zhang, P., McGrath, B., Li, S., Frank, A., Zambito, F., Reinert, J., Gannon, M., Ma, K., McNaughton, K., and Cavener, D. R. (2002). The PERK eukaryotic initiation factor 2 alpha kinase is required for the development of the skeletal system, postnatal growth, and the function and viability of the pancreas. Mol Cell Biol *22*, 3864-3874.

Zhang, S. L., Kozak, J. A., Jiang, W., Yeromin, A. V., Chen, J., Yu, Y., Penna, A., Shen, W., Chi, V., and Cahalan, M. D. (2008). Store-dependent and -independent modes regulating Ca2+ release-activated Ca2+ channel activity of human Orai1 and Orai3. J Biol Chem *283*, 17662-17671.

Zhu, X., Jiang, M., Peyton, M., Boulay, G., Hurst, R., Stefani, E., and Birnbaumer, L. (1996). trp, a novel mammalian gene family essential for agonist-activated capacitative Ca2+ entry. Cell *85*, 661-671.

Zweifach, A., and Lewis, R. S. (1993). Mitogen-regulated Ca2+ current of T lymphocytes is activated by depletion of intracellular Ca2+ stores. Proc Natl Acad Sci U S A *90*, 6295-6299.